

# Nonlinear responses of particulate nitrate to NO<sub>x</sub> emission controls in the megalopolises of China

Mengmeng Li<sup>1,\*</sup>, Zihan Zhang<sup>1</sup>, Tijian Wang<sup>1</sup>, Min Xie<sup>1</sup>, Shu Li<sup>1</sup>, Bingliang Zhuang<sup>1</sup>  
and Yong Han<sup>2</sup>

<sup>1</sup> School of Atmospheric Sciences, Nanjing University, Nanjing 210023, China

<sup>2</sup> Guangdong Province Key Laboratory for Climate Change and Natural Disaster Studies, School of Atmospheric Sciences, Sun Yat-Sen University, Guangzhou, China

\* Corresponding author: mengmengli2015@nju.edu.cn

## Abstract

Nitrate is an increasingly important component of fine particulate matter (PM<sub>2.5</sub>) in Chinese cities. The production of nitrate is not only related to the abundance of its precursor but also supported by the atmospheric photochemical oxidants, raising a new challenge to the current emission control actions in China. This paper uses comprehensive measurements and a regional meteorology-chemistry model with optimized mechanisms to establish the nonlinear responses between particulate nitrate and nitrogen oxides (NO<sub>x</sub>) emission controls in the megalopolises of China. Nitrate is an essential component of PM<sub>2.5</sub> in eastern China, accounting for 9.4–15.5% and 11.5–32.1% of the PM<sub>2.5</sub> mass for the warm and cold seasons. The hypothetical NO<sub>x</sub> emission reduction scenarios (–10%~–80%) during summer-autumn result in almost linearly lower PM<sub>2.5</sub> by –2.18% in Beijing-Tianjin-Hebei (BTH) and –2.89% in Yangtze River Delta (YRD) per 10% cut of NO<sub>x</sub> emissions, whereas they lead to a rather complicated response of PM components in winter. Wintertime nitrate is found to increase by +4.12% in BTH and +5.05% in YRD per 10% cut of NO<sub>x</sub> emissions, with nearly unchanged nitric acid (HNO<sub>3</sub>) and higher dinitrogen pentoxide (N<sub>2</sub>O<sub>5</sub>) intermediate products produced from the increased atmospheric oxidants levels. An

inflexion point appears at 40–50% NO<sub>x</sub> emission reduction, and a further cut in NO<sub>x</sub> emissions is predicted to cause  $-10.49\%$  reduction of nitrate for BTH and  $-7.68\%$  for YRD per 10% cut of NO<sub>x</sub> emissions. In addition, the 2012–2016 NO<sub>x</sub> control strategy actually leads to no changes or even increases of nitrate in some areas (8.82% in BTH and 14.41% in YRD) during winter. Our results also emphasize that ammonia (NH<sub>3</sub>) and volatile organic compounds (VOC<sub>s</sub>) are effective in controlling nitrate pollution, whereas decreasing the sulfur dioxide (SO<sub>2</sub>) and NO<sub>x</sub> emissions may have counter-intuitive effects on nitrate aerosols. This paper helps understand the nonlinear aerosol and photochemistry feedbacks, and defines the effectiveness of proposed mitigations for the increasingly serious nitrate pollution in China.

## 1 Introduction

Secondary inorganic aerosols (SIA), including sulfate ( $\text{SO}_4^{2-}$ ), nitrate ( $\text{NO}_3^-$ ) and ammonium ( $\text{NH}_4^+$ ) account for 30–60% of the total fine particulate matter ( $\text{PM}_{2.5}$ ) mass during haze events in China (Huang et al., 2014a; Zhao et al., 2013). Since the enactment of the Air Pollution Action Plan in 2013, the Chinese government has taken drastic measures to reduce the emissions of sulfur dioxide ( $\text{SO}_2$ ), nitrogen oxides ( $\text{NO}_x$ ) and primary  $\text{PM}_{2.5}$ , leading to significant decreases in sulfate and overall  $\text{PM}_{2.5}$  concentrations in cities (Silver et al., 2018; Li et al., 2021a; Wang et al., 2017b). Meanwhile, the nitrogen/sulfur (N/S) ratio in  $\text{PM}_{2.5}$  increased significantly and nitrate had been the main component of  $\text{PM}_{2.5}$  (16–45%) during haze episodes, despite a more than 20% reduction in the concentrations of its precursor  $\text{NO}_x$  (Shao et al., 2018; Wen et al., 2018; Zhai et al., 2019). The increasingly serious nitrate pollution has emerged to be the new emphasis of air pollution controls in China.

Nitrate formation involves complex multiphase chemical reactions. In the daytime, nitrogen dioxide ( $\text{NO}_2$ ) reacts with hydroxyl radical ( $\text{OH}$ ) to produce nitric acid ( $\text{HNO}_3$ ). With excess ammonium ( $\text{NH}_3$ ), low temperature and insufficient sulphuric acid, this reaction can proceed quickly and produce high ammonium nitrate (Seinfeld and Pandis, 2006). In the nighttime, however, high-concentration  $\text{NO}_2$  reacts with ozone ( $\text{O}_3$ ) to produce the nitrate radical ( $\text{NO}_3$ ) and dinitrogen pentoxide ( $\text{N}_2\text{O}_5$ ). The heterogeneous hydrolysis of  $\text{N}_2\text{O}_5$  on wet particles is the main pathway for nocturnal nitrate formation (56–97%) (He et al., 2018; Pathak et al., 2011; Xue et al., 2014).

Nitrate chemistry is not only related to the abundance of its precursor  $\text{NO}_x$ , but also supported by the atmospheric oxidants (e.g.,  $\text{OH}$  and  $\text{O}_3$ ) produced from the photochemical reactions of  $\text{NO}_x$  and volatile organic compounds ( $\text{VOC}_s$ ) (Meng et al.,

1997). Using a box model, some studies have determined that the relationship between particulate nitrate and  $\text{NO}_x$  emissions is nonlinear depending on the ozone chemical sensitivity regime (Pun and Seigneur, 2001; Nguyen and Dabdub, 2002). Pun and Seigneur (2001) showed that the daytime  $\text{HNO}_3$  production was more sensitive to the concentrations of atmospheric oxidants, and that in the VOC-limited regime the decrease of  $\text{HNO}_3$  production due to the  $\text{NO}_x$  emission control might be offset by the increase of OH. Nguyen and Dabdub (2002) calculated the detailed isopleth between nitrate and  $\text{NO}_x$  emissions; they found that the reduction of  $\text{NO}_x$  emissions resulted in a decrease of nitrate in the  $\text{NO}_x$ -limited regime, and an increase of nitrate under extreme conditions in the VOC-limited regime. Despite that, the single-site box model results could not distinguish the regional differences among chemical regimes; the basic hypotheses in box models to predict nitrate production are also unreasonable in the real atmosphere.

As an important precursor for both fine particles and ozone, the strict control of  $\text{NO}_x$  emissions has started in China since the 12<sup>th</sup> Five-Year Plan (Zheng et al., 2018). A confounding factor is that, for most cities in China, the production of  $\text{O}_3$  is usually limited by  $\text{VOC}_s$  (Xie et al., 2014; Dong et al., 2014; Liu et al., 2010). The control of  $\text{NO}_x$  emissions has therefore resulted in an increase of surface  $\text{O}_3$  concentrations in recent years (Li et al., 2021a; Li et al., 2019a; Kalsoom et al., 2021), implying complex impacts on nitrate formation. Li et al. (2021a) and Liu and Wang (2020) examined the influencing factors on the surface  $\text{O}_3$  trends in China from 2013 to 2017 using regional chemical models. They highlighted that the control of  $\text{NO}_x$  emissions explained 11–35% of the increased  $\text{O}_3$  due to the nonlinear  $\text{NO}_x$ - $\text{VOC}_s$ - $\text{O}_3$  chemistry, and that for most regions the magnitudes could be comparable to those resulting from the meteorological influences and aerosol effects. Some simulations thought that the

NO<sub>x</sub> emission increase in 2005–2012 resulted in an increase of nitrate by 3.4% yr<sup>-1</sup> in eastern China (Geng et al., 2017; Wang et al., 2013), and the following NO<sub>x</sub> emission control resulted in a decrease of nitrate by 3–14% (Wang et al., 2014). Recent evidence from field observations (Fu et al., 2020) and numerical simulations (Dong et al., 2014), however, suggested that the NO<sub>x</sub> emission reduction in China could result in an increase of nitrate in winter through increased photochemical oxidants and nocturnal N<sub>2</sub>O<sub>5</sub> chemistry, but a decrease in other seasons. In the next 5–10 years, SO<sub>2</sub> emissions might level off in China, while NO<sub>x</sub> emissions will become stringently controlled to ensure further air quality improvements (Zheng et al., 2018). Accurately understanding the nonlinear aerosol and photochemistry feedbacks is crucial to resolve the emerging nitrate pollution and to establish reasonable air pollution control strategies in China.

To address this issue, we use comprehensive measurements and a regional meteorology-chemistry model combined with hypothetical NO<sub>x</sub> emission scenarios to establish the nonlinear response relationships between particulate nitrate and NO<sub>x</sub> emission controls in the megalopolises of China. The model configurations, numerical designs and observational data are presented in Sect. 2. Sect. 3 discusses the results. Finally, a summary is presented in Sect. 4.

## 2 Materials and Methods

### 2.1 Model setup and experimental designs

This study uses the Weather Research and Forecasting-Chemistry (WRF-Chem) model version 4.1 developed by Grell et al. (2002) to simulate the regional meteorology and atmospheric chemistry. The mesoscale meteorology and air quality simulations of WRF-Chem have been improved in terms of incorporating the satellite-derived land surface parameters (Li et al., 2014; Li et al., 2017), and optimizing the

SIA formation pathways enhanced by mineral aerosols (Li et al., 2019b; Huang et al., 2014b).

The modeling domain covers two main megalopolises of China and its adjacent areas—the Beijing-Tianjin-Hebei (BTH) region and the Yangtze River Delta (YRD) region (Fig. 1). The modeling framework is configured with 81×86 grid cells at 25 km horizontal resolution. The model is run with an 84-hour model cycle, with the first 12 hours discarded as spin-up time and model outputs of each model cycle to provide chemical initial conditions for the subsequent overlapping 84-hour simulation. The 6-hour, 1°×1° National Centers for Environmental Prediction Final (NCEP/FNL) analysis fields are regularly input for the model initial and lateral boundary meteorological conditions.

The model physical configurations include the YSU boundary layer scheme (Noh et al., 2003), the RRTMG radiation scheme (Iacono et al., 2008), the Noah land surface scheme (Ek et al., 2003) and the Lin microphysics scheme (Lin et al., 1983). We **have updated** the land cover type and vegetation data in WRF mesoscale model with the latest land surface parameters derived from Moderate Resolution Imaging Spectroradiometer (Li et al., 2014; Li et al., 2017).

The atmospheric chemistry is simulated using the Carbon Bond Mechanism version Z (CBMZ) (Zaveri and Peters, 1999) gas-phase chemistry module coupled with a four-bin sectional Model for Simulating Aerosol Interactions and Chemistry (MOSAIC) (Zaveri et al., 2008). The aqueous-phase chemistry is based on the Carnegie Mellon University (CMU) scheme including 50 species and more than 100 reactions (Fahey and Pandis, 2001). Formation of SIA in the **default WRF-Chem model** accounts for the gas-phases oxidation of SO<sub>2</sub> and NO<sub>2</sub>, and aqueous-phase oxidation of SO<sub>2</sub> by hydrogen peroxide (H<sub>2</sub>O<sub>2</sub>) and O<sub>3</sub> in cloud. We **have optimized**

the SIA formation pathways by including the aqueous SO<sub>2</sub> oxidation catalyzed by mineral ions and heterogeneous uptakes of SO<sub>2</sub>, NO<sub>2</sub>, NO<sub>3</sub>, N<sub>2</sub>O<sub>5</sub> and HNO<sub>3</sub> on mineral aerosols in the MOSAIC aerosol module (Li et al., 2019b; Huang et al., 2014b).

Anthropogenic emissions are adopted from the 2016 Multi-resolution Emission Inventory for China (MEIC) and the 2010 MIX-Asia emission inventory for regions outside of mainland China developed by Tsinghua University (<http://meicmodel.org>). Biogenic emissions are calculated online using the Model of Emissions of Gases and Aerosols from Nature (Guenther et al., 2006).

A series of WRF-Chem simulations is designed as summarized in Table 1. In the baseline simulation (denoted as the B0 scenario), the anthropogenic emissions in China remain unchanged at the usual levels in 2016. Simulation N0 is the same as B0, but it only considers the gas-phase oxidation production of HNO<sub>3</sub> (NO<sub>2</sub>+OH→HNO<sub>3</sub>) and its subsequent partitioning to the aerosol phase of nitrate in WRF-Chem. The B0 and N0 simulations are combined to distinguish the contributions of gas-phase oxidation and heterogeneous pathways (i.e., uptakes of N<sub>2</sub>O<sub>5</sub>, NO<sub>3</sub> and NO<sub>2</sub>) for the formation of nitrate aerosols during the warm and cold seasons. A group of sensitivity scenarios (C1~C8) are designed with the perturbed anthropogenic NO<sub>x</sub> emissions in China cut by 10%, 20%...and 80%, respectively. The differences between B0 and C1~C8 simulations are calculated to illustrate the responses of particulate pollution in China's megacities to the NO<sub>x</sub> emission reduction scenarios. Another simulation (E1) is designed with the anthropogenic emissions of NO<sub>x</sub> in China set to the 2012 levels to show the impacts of 2012–2016 NO<sub>x</sub> control strategy on particulate pollution. Additionally, in order to evaluate the effectiveness of multi-pollutants cooperative controls, three series of simulations (C<sub>S-N</sub>, C<sub>N-N</sub> and C<sub>V-N</sub>) are also supplemented with

the anthropogenic emissions of SO<sub>2</sub>, NH<sub>3</sub> and VOC<sub>s</sub> in China cut by 20%, 40%...and 80%, respectively. The differences between B0 and C<sub>N</sub>/C<sub>S-N</sub>/C<sub>N-N</sub>/C<sub>V-N</sub> simulations are calculated to illustrate the responses of nitrate pollution in China's megacities to the multi-pollutants cooperative controls.

For all simulation scenarios, two month-long periods during the Campaign on Air Pollution and Urban Meteorology in Yangtze River Delta (CAPUM-YRD)—August 15 to September 16 (Period I) and November 24 to December 26 (Period II) in 2016, are simulated to represent the warm and cold seasons, respectively (Shu et al., 2019). The complete simulation consists of thirteen 84-hour model cycles with the first 6 days as spin-up for chemistry and the remaining model outputs for analysis.

## 2.2 Weather and air pollutants data

Surface meteorological observations at 186 land-based automatic stations across China (Fig. 1) are collected for model meteorological validation, including hourly data of 2 m air temperature, 2 m relative humidity and 10 m wind speed. These data are archived at the U. S. National Climatic Data Center (NCDC) (Smith et al., 2011).

Air pollutants data at the national air quality monitoring network and regional supersites of China (Fig. 1) are used for model chemical validation. This nationwide monitoring network contains 1597 sites covering 454 cities in mainland China, as shown in Fig. 1. Six routine air pollutants including PM<sub>2.5</sub>, particulate matter with aerodynamic diameter less than 10 μm (PM<sub>10</sub>), SO<sub>2</sub>, NO<sub>2</sub>, carbon monoxide (CO) and O<sub>3</sub> are monitored and reported hourly by Chinese National Environmental Monitoring Center (CNEMC) network (available at <http://websearch.mep.gov.cn/>).

Additionally, four comprehensive atmospheric environment supersites in YRD including Dianshanhu (DSH; 31.1°N, 121.0°E), Pudong (PD; 31.2° N, 121.5°E), Nanjing (NJ; 32.1°N, 118.8°E) and Hangzhou (HZ; 30.3°N, 120.2°E) measured the



mass concentrations of PM<sub>2.5</sub>, water-soluble ions (sulfate, nitrate, ammonium, sodium, chloride, potassium, calcium and magnesium), carbonaceous aerosols (elemental carbon (EC) and organic carbon (OC)) and gaseous pollutants (SO<sub>2</sub>, NO<sub>2</sub>, CO and O<sub>3</sub>) during the CAPUM-YRD campaign. Details for the methods and data at the four supersites are described in Shu et al. (2019).

### 3 Results and discussions

#### 3.1 Model weather and chemical validation

Model evaluations indicate that the WRF-Chem model is able to simulate the weather and atmospheric pollution characteristics in China. The simulated magnitudes of surface temperature by WRF-Chem in general agree with actual observations, with a correlation efficient (*R*) of 0.89 and 0.94, and a normalized mean bias (NMB) of −0.55% and −0.80% respectively in Period I and Period II (Table 2). Underestimation of relative humidity (−5.65% in Period I and −6.56% in Period II) is common in the WRF simulation and it might be attributed to the influence of the boundary layer parameterization on the weather forecast (Bhati and Mohan, 2018; Gomez-Navarro et al., 2015). Clear overestimation of wind speed (23.72% in Period I and 40.64% in Period II) might be because of the unresolved topography in WRF (Jimenez et al., 2013; Li et al., 2014).

The predicted concentrations of routine air pollutants also faithfully capture the spatial and seasonal patterns of observed surface PM<sub>2.5</sub>, SO<sub>2</sub>, NO<sub>2</sub> and O<sub>3</sub> levels in both seasons (Fig. 2). Both simulations and observations display high air pollutants concentrations in the vicinity of North China Plain (NCP) and eastern China, but with higher O<sub>3</sub> levels in the warm season and oppositely higher PM<sub>2.5</sub> and other gaseous pollutants concentrations in winter. The model statistical evaluations show a mean bias (MB) of −3.66, −1.14, 4.7 and 18.32 μg m<sup>−3</sup>, and NMB of −9.92, −6.46, 16.47

and 7.72% for PM<sub>2.5</sub>, SO<sub>2</sub>, NO<sub>2</sub> and O<sub>3</sub> in Period I, and a relatively larger MB of −27.31, −11.65, 1.27 and −39.01  $\mu\text{g m}^{-3}$ , and NMB of −29.82, −28.11, 2.40 and −31.05% in Period II, respectively (Table 3). The uncertainty in emissions data, the absence of secondary organic aerosol in MOSAIC aerosol chemistry or the simulated wind errors (Table 2) may be responsible for the larger atmospheric chemical biases in winter, which has been extensively discussed in some studies (Zhao et al., 2016; Li et al., 2021a).

As the most important components of PM<sub>2.5</sub>, reasonable representation of SIA is imperative to PM<sub>2.5</sub> simulation. Evaluations with measurements of PM<sub>2.5</sub> components at the four supersites of eastern China show that the model performs reasonably in simulating the seasonal variations and proportions of aerosol species in PM<sub>2.5</sub>, but it is biased low by 10–40% in simulating the magnitudes of SIA concentrations (Fig. 3). The model underestimation is −1.8, −2.2 and −2.2  $\mu\text{g m}^{-3}$  for sulfate, nitrate and ammonium, respectively, in Period I, and −2.6, −4.3 and −3.4  $\mu\text{g m}^{-3}$  in Period II. The model also captures the large change of N/S ratio from the warm to cold seasons, that increases from 0.42 in Period I to 1.56 in Period II. Our previous work (Li et al., 2019) has confirmed that the consideration of the optimized aqueous and heterogeneous SIA formation pathways in WRF-Chem significantly reduces the model biases by 41.38% for sulfate and 44.55% for nitrate during the CAPUM-YRD campaign of 2016. Recent studies highlighted that the remaining SIA simulation biases may be attributed to the missing aqueous oxidation of SO<sub>2</sub> by NO<sub>2</sub> on alkaline aerosols under humid conditions (Wang et al., 2016; Cheng et al., 2016).

### 3.2 Air pollution and aerosol composition characteristics

Chemical composition analyses of major gaseous and particulate air pollutants suggest large seasonal variations of air pollution characteristics in China (Fig. 2).

Mainly emitted from combustion sources, atmospheric pollutants accumulate in the densely industrialized and populated megalopolises of China, with a hotspot along Beijing, Hebei, Shandong and their adjacent cities frequently exceeding China's National Ambient Air Quality Standards. The average concentrations of surface PM<sub>2.5</sub>, SO<sub>2</sub>, NO<sub>2</sub> and daily-maximum O<sub>3</sub> in China's routine air quality monitoring network are 36.88, 17.65, 28.53 and 237.45 µg m<sup>-3</sup> for Period I, and 91.59, 41.45, 53.01 and 125.62 µg m<sup>-3</sup> for Period II. The surface PM<sub>2.5</sub>, SO<sub>2</sub> and NO<sub>2</sub> concentrations show obvious increases by 148.35%, 134.84% and 85.80% during winter compared to those of the summer-autumn period (Period I). The maximum surface PM<sub>2.5</sub> concentrations recorded in the winter period was more than 600 µg m<sup>-3</sup>, which is the highest value ever recorded in 2016 and leads to the "orange" air quality alert.

The further analyses of PM<sub>2.5</sub> mass concentrations, major PM<sub>2.5</sub> components and gases at the four supersites in YRD are presented in Fig. 4–5. Organic matter (OM) is obtained by multiplying the OC concentrations by a factor of 1.6, mainly accounting for the hydrogen and oxygen masses in OM. The measured SIA concentrations exhibit high levels, with average values of 18.8 µg m<sup>-3</sup> for Period I and 37.1 µg m<sup>-3</sup> for Period II. The three SIA components together account for 32.3–57.4% (48.6% on average) and 27.7–70.9% (56.9% on average) of the total PM<sub>2.5</sub> mass concentrations, and become the primary components of PM<sub>2.5</sub> in the two periods. The proportions of sulfate, nitrate and ammonium in total PM<sub>2.5</sub> range from 13.5–28.9%, 9.4–15.5% and 9.4–14.9% at the four supersites for Period I, and 9.2–20.3%, 11.5–32.1% and 7.0–19.8% for Period II, respectively. The strikingly higher proportion of nitrate than that of sulfate in PM<sub>2.5</sub> during winter, with a N/S ratio of 1.56, is in accordance with recent observations during other winter haze periods in China (Shao et al., 2018; Zhang et al., 2018; Zhang et al., 2019). They emphasized that since the enactment of Clean Air

Action Plan in 2013, the PM<sub>2.5</sub> components had changed clearly with decreasing contributions from coal combustion.

The high proportions of sulfate and nitrate in PM<sub>2.5</sub> could be related to the high oxidation rates of SO<sub>2</sub> and NO<sub>2</sub>. The observed average values of sulfur oxidation ratio ( $SOR = [SO_4^{2-}] / ([SO_4^{2-}] + [SO_2])$ ) and nitrogen oxidation ratio ( $NOR = [NO_3^-] / ([NO_3^-] + [NO_2])$ ) are 0.41 and 0.13 in Period I, and 0.33 and 0.21 in Period II. In contrast, the observed SOR is generally higher in summer-autumn than winter, opposite to that of NOR, indicating the enhanced formation of nitrate in winter. Shu et al. (2019) also noted similar seasonal distinctions for SOR and NOR in YRD. They attributed the weakened conversion from NO<sub>2</sub> to nitrate in summer to the volatility and evaporative loss of nitrate (Sun et al., 2012). The sharp increase of particles and moderate ambient humidity in winter also benefit the heterogeneous formation of SIA, leading to high NOR and SOR (Wang et al., 2012).

Figure 6 illustrates the contributions of gas-phase oxidation and heterogeneous reactions for the nitrate production calculated from B0 and E0 simulations. It is shown that on a daily basis the gas-phase oxidation production of HNO<sub>3</sub> and its subsequent partitioning to the aerosol phase is the principal formation route for particulate nitrate, with the average contributions of 60.19% for BTH and 91.71% for YRD in Period I and 75.14% for BTH and 85.94% for YRD in Period II. The heterogeneous hydrolyses of N<sub>2</sub>O<sub>5</sub> and other nitrogenous gases (calculated as the model differences between B0 and N0 simulations) contribute to the remaining nitrate, particularly in BTH with high aerosol loading. These calculated results (60.19–91.71% for NO<sub>2</sub>+OH oxidation and 8.29–39.81% for heterogeneous pathways) are in line with previous assessments in China and globally. Alexander et al. (2009) reported that the global tropospheric nitrate burden is dominated by NO<sub>2</sub>+OH (76%), followed by N<sub>2</sub>O<sub>5</sub>

hydrolysis (18%); but recent results suggested that  $\text{N}_2\text{O}_5$  hydrolysis was as important as  $\text{NO}_2 + \text{OH}$  (both 41 %) for global nitrate production (Alexander et al., 2020). In major Chinese cities, it was estimated that the conversion of  $\text{NO}_x$  to nitrate was dominated by  $\text{NO}_2 + \text{OH}$  oxidation in Shanghai, with a mean contribution of 55–77% in total and even higher (84–92%) in summer (He et al., 2020). In NCP, the nitrate contribution of heterogeneous pathways was about 30.8% (Liu et al., 2020) or even comparable to the partitioning of  $\text{HNO}_3$  (Wang et al., 2019; Wang et al., 2017a; Luo et al., 2021). The nitrate formation from heterogeneous pathways is moderately underestimated in the optimized WRF-Chem model of this study, possibly due to the uncertainties of heterogeneous uptake coefficients and unclear reaction mechanisms applied in the model (Li et al., 2019b; Xue et al., 2016; He et al., 2014).

### 3.3 Nonlinear responses of **nitrate** to $\text{NO}_x$ emissions and their policy **implications**

#### 3.3.1 $\text{PM}_{2.5}$ - $\text{NO}_x$ and $\text{O}_3$ - $\text{NO}_x$ responses in the warm and cold seasons

$\text{NO}_x$  is key in atmospheric chemistry and serves as an important precursor for both ozone and secondary aerosols. We conduct a series of simulations (C1~C8) with perturbed  $\text{NO}_x$  emissions to assess the responses of  $\text{PM}_{2.5}$  mass concentrations to  $\text{NO}_x$  emissions in two megalopolises of China (Fig. 7). The WRF-Chem simulation results show that the responses of surface  $\text{PM}_{2.5}$  concentrations to  $\text{NO}_x$  emissions vary in different seasons and display strong **nonlinear behaviour** in winter. To better quantify their effectiveness, we define the  $\text{NO}_x$  emission control efficiency ( $\beta$ ), **which denotes** the percentage **changes** of **surface**  $\text{PM}_{2.5}$  or its components concentrations in response to **the** successive 10% cut of  $\text{NO}_x$  **emissions**.

In Period I (Aug–Sep), the  $\text{PM}_{2.5}$ - $\text{NO}_x$  responses are closer to a linear function, reflecting a stronger sensitivity to **the**  $\text{NO}_x$  emission changes in the warm season. The surface  $\text{PM}_{2.5}$  concentrations decrease almost linearly as we gradually reduce  $\text{NO}_x$

emissions in China, with the average  $\beta$  values of  $-2.18\%$  in BTH and  $-2.89\%$  in YRD. However, the  $\text{PM}_{2.5}$ - $\text{NO}_x$  emission responses in Period II (Nov–Dec) display strong nonlinearity and are analogous to a quadratic parabola distribution for both regions. The  $\text{NO}_x$  emission reductions within the first 50% would even increase surface  $\text{PM}_{2.5}$  concentrations by  $+1.25\%$  averagely in BTH, and this  $\beta$  value increases to  $+1.76\%$  in YRD with the first 40% reductions of  $\text{NO}_x$  emissions. Subsequently, the  $\text{PM}_{2.5}$  responses shift towards a similar linear pattern, with an average  $\beta$  value of  $-2.51\%$  in BTH and  $-3.96\%$  in YRD.

The distinct forms of  $\text{PM}_{2.5}$ - $\text{NO}_x$  emission responses for the warm and cold seasons are determined by the seasonal ozone chemical sensitivity regimes. The photochemical indicator of  $\Delta[\text{O}_3]_{\text{NO}_x}/\Delta[\text{O}_3]_{\text{VOC}_s}$  with a critical value of 1.0 is used to investigate the season-varying ozone sensitivity in China, which is calculated as the ratio of ozone concentration changes under 20%  $\text{NO}_x$  emission reduction to that under 20%  $\text{VOC}_s$  emission reduction (Fig. S1). The results indicate a strong VOC-limited ozone chemistry across China during winter, while either VOC-limited regime over a large portion of NCP and eastern China or  $\text{NO}_x$ -limited regime in northern and western China during summer-autumn, as also indicated from previous studies (Xie et al., 2014; Dong et al., 2014; Liu et al., 2010). We find larger  $\text{O}_3$  and OH productions under the  $\text{NO}_x$  emission reduction conditions in both seasons (Fig. 8–9), particularly in Period II (Nov–Dec) with an average increase rate of  $+14.72\%$  and  $+18.50\%$  in BTH and  $+25.17\%$  and  $+23.09\%$  in YRD per 10% cut of  $\text{NO}_x$  emissions. The SIA formation chemistry is highly limited by atmospheric oxidants produced from the  $\text{NO}_x$ - $\text{VOC}_s$ - $\text{O}_3$  photochemical cycles. The nonlinear  $\text{O}_3$ - $\text{NO}_x$  responses indicate a rather complicated aerosol and photochemistry feedback in megacities.

### 3.3.2 Nonlinear responses of particulate nitrate to NO<sub>x</sub> emissions

The SIA formation is basically driven by the atmospheric oxidants levels, and a reduction of NO<sub>x</sub> emissions may have counter-intuitive effects on SIA components by controlling the atmospheric oxidants levels. The calculated SIA components for each emission scenario in both months show that the surface nitrate aerosols can be substantially decreased/increased with reducing NO<sub>x</sub> emissions, but the sulfate and ammonium concentrations have moderately smaller changes (Fig. 8–10).

Response of sulfate to the NO<sub>x</sub> emissions is more predictable and determined by the changes of atmospheric oxidants levels since that the conversion of SO<sub>2</sub> to sulfate is partly driven by OH in the gas-phase and by dissolved H<sub>2</sub>O<sub>2</sub> or O<sub>3</sub> in the presence of fog or cloud. In Period I (Aug–Sep), the sulfate-NO<sub>x</sub> response follows a gradual quadratic parabola distribution as that of O<sub>3</sub>-NO<sub>x</sub> and OH-NO<sub>x</sub> response curves (Fig. 8 and Fig. 10), with a fitted function in Eq. 1. The  $\beta$  values for surface sulfate change by  $-0.74\%\sim+1.16\%$  in BTH and  $-1.54\%\sim+0.17\%$  in YRD under the  $-10\sim-80\%$  NO<sub>x</sub> emission reduction scenarios.

$$[\text{SO}_4^{2-}] = -2.45\Delta\text{E}_{\text{NO}_x}^2 - 2.15\Delta\text{E}_{\text{NO}_x} + 5.90 \text{ in BTH } (R^2=0.9309) \quad (\text{Eq. 1})$$

$$[\text{SO}_4^{2-}] = -2.26\Delta\text{E}_{\text{NO}_x}^2 - 1.31\Delta\text{E}_{\text{NO}_x} + 6.65 \text{ in YRD } (R^2=0.9893)$$

where  $[\text{SO}_4^{2-}]$  is the surface mean concentration of sulfate ( $\mu\text{g m}^{-3}$ );  $\Delta\text{E}_{\text{NO}_x}$  is the percentage change of NO<sub>x</sub> emissions (%).

As expected, the production of nitrate reflects a strong sensitivity to NO<sub>x</sub> and it decreases linearly with the NO<sub>x</sub> emission control, with an average  $\beta$  value of  $-10.21\%$  in BTH and  $-11.51\%$  in YRD, which further leads to a decrease of ammonium concentrations by  $-3.25\%$  in BTH and  $-4.35\%$  in YRD (Fig. 8 and Fig. 10). The formation of nitrate mainly involves the  $\text{NO}_2 + \text{OH} \rightarrow \text{HNO}_3$  gas-phase oxidation and the heterogeneous hydrolysis of  $\text{N}_2\text{O}_5$  and other nitrogenous gases. The strong

sensitivity of particulate nitrate in response to the  $\text{NO}_x$  emission decreases can be explained by the synchronously suppressive production of its intermediate products  $\text{HNO}_3$  and  $\text{N}_2\text{O}_5$ . For example, when the  $\text{NO}_x$  emission is cut by 20%, the surface  $\text{NO}_2$  concentration in BTH drops by 21.96% but the surface  $\text{O}_3$  and OH concentrations increase slightly by 2.56% and 5.28% due to the reduction of  $\text{NO}+\text{O}_3$  titration reaction and the greater VOC availability in the warm season, leading to substantial reductions in surface  $\text{HNO}_3$  (−16.72%) and  $\text{N}_2\text{O}_5$  (−8.94%) concentrations.

$$[\text{NO}_3^-] = -34.54\Delta E_{\text{NO}_x}^2 - 30.66\Delta E_{\text{NO}_x} + 10.52 \text{ in BTH} \quad (R^2=0.8379) \quad (\text{Eq. 2})$$

$$[\text{NO}_3^-] = -36.53\Delta E_{\text{NO}_x}^2 - 26.94\Delta E_{\text{NO}_x} + 9.70 \text{ in YRD} \quad (R^2=0.9862)$$

$$[\text{NH}_4^+] = -9.12\Delta E_{\text{NO}_x}^2 - 8.73\Delta E_{\text{NO}_x} + 5.40 \text{ in BTH} \quad (R^2=0.7759) \quad (\text{Eq. 3})$$

$$[\text{NH}_4^+] = -10.55\Delta E_{\text{NO}_x}^2 - 8.36\Delta E_{\text{NO}_x} + 4.58 \text{ in YRD} \quad (R^2=0.9762)$$

where  $[\text{NO}_3^-]$  and  $[\text{NH}_4^+]$  are the surface mean concentrations ( $\mu\text{g m}^{-3}$ ) of nitrate and ammonium, respectively.

In Period II (Nov–Dec), we find opposite results with quadratic parabola distributions for nitrate- $\text{NO}_x$  response (Eq. 2) and ammonium- $\text{NO}_x$  response (Eq. 3), but linearly increasing sulfate concentrations (average  $\beta$  values of +2.00% in BTH and +2.64% in YRD; Fig. 9 and Fig. 10), leading to small  $\text{PM}_{2.5}$  changes in winter. Such nonlinear nitrate- $\text{NO}_x$  responses can be explained by the substantially increased oxidants as we gradually reduce  $\text{NO}_x$  emissions in each scenario. It is noted that in winter the nitrate- $\text{NO}_x$  response highly depends on the production of  $\text{N}_2\text{O}_5$ , which is produced from the  $\text{NO}_2 \xrightarrow{\text{O}_3} \text{NO}_3 \xrightarrow{\text{NO}_2} \text{N}_2\text{O}_5$  chemical reactions and is a crucial intermediate product for nitrate formation. Under the low  $\text{NO}_x$  emission reduction conditions, the production of  $\text{N}_2\text{O}_5$  is more sensitive to the atmospheric oxidants concentrations. The significant increases of surface  $\text{O}_3$  in each  $\text{NO}_x$  emission scenario in the VOC-poor



environment (Fig. 9(b, d)) lead to an enhancement of  $\text{N}_2\text{O}_5$  levels from 10% to more than 100%. In spite of the  $\text{HNO}_3$  concentration remaining nearly unchanged or decreasing slightly by less than 5% in response to  $\text{NO}_x$  control, nitrate is found to increase (average  $\beta$  values of +4.12% in BTH and +5.05% in YRD) with higher  $\text{N}_2\text{O}_5$  produced from the increased ozone introduced by attenuated titration. An inflexion point appears at the 40–50%  $\text{NO}_x$  emission reduction scenario, and a further reduction in  $\text{NO}_x$  emissions is predicted to cause –10.49% and –5.31% reductions of surface particulate nitrate and ammonium for BTH, and –7.68% and –7.36% for YRD.

These results reveal that the increase in atmospheric oxidants in response to  $\text{NO}_x$  emission control can offset the decreasing precursors concentrations and further enhance the formation of secondary nitrate, as recently found during the COVID-19 pandemic (Huang et al., 2020; Li et al., 2021b).

### 3.3.3 Impacts of 2012–2016 $\text{NO}_x$ control strategy on particulate pollution

During the 12<sup>th</sup> Five-Year Plan period (2011–2015), a series of end-of-pipe pollutant controls (e.g., Selective Catalytic Reduction techniques) were carried out for power, industry and transportation sectors. These measures effectively controlled the national  $\text{NO}_x$  emissions by 22.8% from 2012 to 2016 (MEIC v1.3) in China. To quantify the effects of recent  $\text{NO}_x$  control measures on the levels of photochemical oxidants and particulate nitrate, we conduct an additional simulation with  $\text{NO}_x$  emissions set to the levels of 2012 in E1.

The model simulations (Fig. 11) suggest that reducing China's  $\text{NO}_x$  emissions alone from 2012 to 2016 leads to an average –24.93%~–8.62% decrease of  $\text{NO}_x$  concentrations in the surface layer. As previously pointed out, the 2012–2016  $\text{NO}_x$  emission control measures lead to increased  $\text{O}_3$  and OH levels in winter, which offset the effectiveness of  $\text{NO}_x$  emission reduction in alleviating winter nitrate. No obvious

declines in the winter nitrate levels are observed and even **increases** in some areas (+8.82% in BTH and 14.41% in YRD; **Fig. S2–S3**). As shown, the largest PM<sub>2.5</sub> responses shift towards the southern Hebei and central China provinces, where the wintertime PM<sub>2.5</sub> concentrations are particularly high in this region. The substantial emission changes from 2012 to 2016 lower the PM<sub>2.5</sub> air pollution by up to –1.84% in BTH and –3.52% in YRD for Period I and oppositely increase **the surface** PM<sub>2.5</sub> by 2.36% in BTH and 4.67% in YRD for Period II. The past NO<sub>x</sub> emission control strategy leads to increased **atmospheric oxidants** levels and **deteriorated** particulate pollution in winter due to the nonlinear photochemistry and aerosol chemical feedbacks, without regard to the other **emission** control measures. This conclusion is also supported by evidence from the recent field observations (Fu et al., 2020).

### **3.3.4 Responses of particulate nitrate to multi-pollutants cooperative controls**

**In order to evaluate the effectiveness of multi-pollutants cooperative controls in China, three series of additional simulations ( $C_{S-N}$ ,  $C_{N-N}$  and  $C_{V-N}$ ) are also designed to show the responses of nitrate and PM<sub>2.5</sub> pollution to the emission controls of NO<sub>x</sub>, SO<sub>2</sub>, NH<sub>3</sub> and VOCs, respectively. The results (Fig. 12) show that atmospheric NH<sub>3</sub> and VOCs are effective in controlling the particulate nitrate pollution for both seasons, whereas decreasing the SO<sub>2</sub> and NO<sub>x</sub> emissions may have counter-intuitive effects on the concentration levels of nitrate aerosols.**

Atmospheric NH<sub>3</sub> acts as a critical neutralizing species for SIA production and efficient haze mitigation (Liu et al., 2019). **According to the WRF-Chem simulation, reduction of NH<sub>3</sub> emissions may be effective in reducing the nitrate component, with an average  $\beta$  value of –9.96% in BTH and –10.35% in YRD for Period I, and –8.32% in BTH and –11.47% in YRD for Period II, primarily by suppressing the ammonium nitrate formation. Quantitatively, a 10% reduction in NH<sub>3</sub> emissions can alleviate the**

PM<sub>2.5</sub> pollution by −2.67% during summer-autumn and −3.21% during winter in the two Chinese megacities. Atmospheric chemistry modeling by Wen et al. (2021) also indicated that controlling NH<sub>3</sub> emissions in Beijing would significantly reduce the population-weighted PM<sub>2.5</sub> concentrations by 6.2–21% with 60–100% NH<sub>3</sub> reductions in January, implying the need to consider NH<sub>3</sub> emission controls when designing the PM<sub>2.5</sub> pollution mitigation strategies.

VOC<sub>s</sub>, which is not a direct precursor for SIA, is effective in SIA controls due to their influences on the atmospheric oxidation cycles (Tsimpidi et al., 2008; Womack et al., 2019; Nguyen and Dabdub, 2002). Our results suggest that decreasing VOC<sub>s</sub> emissions per 10% would suppress the oxidation formation of nitrate and decrease the nitrate concentrations by −2.48% in BTH and −1.69% in YRD for Period I, and −5.01% in BTH and −6.35% in YRD for Period II. The reduction of VOC<sub>s</sub> emissions would result in a decrease of PM<sub>2.5</sub> by −0.70% during summer-autumn and −1.76% during winter in the two megacities. Tsimpidi et al. (2008) also showed that the reduction of VOC<sub>s</sub> emissions caused a marginal increase of PM<sub>2.5</sub> during summer in eastern United States, whereas it resulted in a decrease of atmospheric oxidant levels and 5–20% reduction of both inorganic and organic PM<sub>2.5</sub> components during winter. Larger and synchronized NO<sub>x</sub> and VOC<sub>s</sub> emissions controls are required to overcome the adverse effects of nonlinear photochemistry and aerosol chemical feedbacks.

The SO<sub>2</sub> emission reduction, although effective in reducing sulfate and PM<sub>2.5</sub>, is not successful in regulating the nitrate pollution due to the chemical competition in nitrate and sulfate formations (Geng et al., 2017; Wang et al., 2013). Changes in nitrate concentration are linearly associated with the SO<sub>2</sub> emission reductions, with the average  $\beta$  values of 2.90% during summer-autumn and 1.35% during winter. Decreasing SO<sub>2</sub> emissions is less effective (a  $\beta$  value of −0.74%) in mitigating the

wintertime haze pollution because that the benefit of SO<sub>2</sub> reduction is partly offset by the significant increase of nitrate, demonstrating the critical role of multi-pollutants cooperative controls. Lei et al. (2013) evaluated the impacts of SO<sub>2</sub> control strategies on nitrate and sulfate production in USA and also found that the competition for bases in nitrate and sulfate formation significantly affects the nitrate concentrations.

Our results emphasize that future nitrate and PM<sub>2.5</sub> pollution mitigation strategies should focus on reducing the chemical precursors and key atmospheric oxidants involved in the production of secondary aerosols. The recent “Three-year Action Plan Fighting for a Blue Sky” calls for stringent emissions controls of NO<sub>x</sub>, SO<sub>2</sub>, VOC<sub>s</sub> and NH<sub>3</sub> but without specific reduction targets. Such emission changes would emphasize the need to jointly consider multi-pollutants emissions controls for mitigating haze air pollution.

#### 4 Conclusions

Recent air pollution actions have significantly lowered the PM<sub>2.5</sub> levels in China via controlling emissions of SO<sub>2</sub> and NO<sub>x</sub>, but raised a new question of how effective the NO<sub>x</sub> emission controls can be on the mitigation of emerging nitrate and ozone air pollution. We use comprehensive measurements and a regional meteorology-chemistry model with optimized mechanisms to establish the nonlinear responses between particulate nitrate and NO<sub>x</sub> emission controls in the megalopolises of China.

Nitrate is an essential component of PM<sub>2.5</sub> in eastern China, accounting for 9.4–15.5% and 11.5–32.1% of the total PM<sub>2.5</sub> mass for the warm and cold seasons, respectively. We find that the efficiency of PM<sub>2.5</sub> reduction is highly sensitive to NO<sub>x</sub> emissions and it varies in different seasons depending on the ozone chemical regimes. The reduction of NO<sub>x</sub> emissions results in almost linearly lower PM<sub>2.5</sub> by −2.18% in BTH and −2.89% in YRD per 10% cut of NO<sub>x</sub> emissions during summer-autumn,

whereas it increases the atmospheric oxidants levels and leads to a rather complicated response of the PM components in winter. Nitrate is found to increase (average  $\beta$  values of +4.12% in BTH and +5.05% in YRD) in winter with higher  $\text{N}_2\text{O}_5$  intermediate produced from the increased ozone introduced by attenuated titration, despite the nearly unchanged or slightly decreased  $\text{HNO}_3$  concentrations in response to  $\text{NO}_x$  control. An inflexion point appears at 40–50%  $\text{NO}_x$  emission reduction, and a further reduction of  $\text{NO}_x$  emissions is predicted to cause –10.49% reductions of particulate nitrate for BTH and –7.68% for YRD. In addition, the 2012–2016  $\text{NO}_x$  emission control strategy leads to –24.93%~–8.62% decreases of surface  $\text{NO}_x$  concentrations, and no changes or even increases of wintertime nitrate in BTH (+8.82%) and YRD (14.41%). Our results also emphasize that atmospheric  $\text{NH}_3$  and VOCs are effective in controlling the particulate nitrate pollution, whereas decreasing the  $\text{SO}_2$  and  $\text{NO}_x$  emissions may have counter-intuitive effects on nitrate aerosols. These results provide insights for developing mitigation strategies for the ubiquitous nitrate aerosols in winter haze of China.

#### Author contribution

Mengmeng Li developed the model code, designed the numerical experiments, and wrote the original draft. Zihan Zhang carried out the numerical experiments. Min Xie, Shu Li and Bingliang Zhuang validated and analyzed the model results. Tijian Wang and Yong Han reviewed and revised the manuscript.

#### Competing interests

The authors declare that they have no conflict of interest.

#### Acknowledgement

This study is funded by the National Natural Science Foundation of China (41975153, 42077192 and 41775056), the National Key Basic Research Development

Program of China (2019YFC0214603, 2020YFA0607802), and the Emory University-Nanjing University Collaborative Research Grant.

## **Data availability statement**

The WRF-Chem model version 4.1 is available at <http://www2.mmm.ucar.edu/wrf/users/downloads.html>. The NCEP FNL data are accessible at the National Center for Atmospheric Research (NCAR) Research Data Archive (RDA; <http://rda.ucar.edu/datasets/ds083.2/>). The MEIC anthropogenic emission inventories are available at [www.meicmodel.org](http://www.meicmodel.org), and for more information, please contact Q. Zhang ([qiangzhang@tsinghua.edu.cn](mailto:qiangzhang@tsinghua.edu.cn)). The surface weather data are accessible at the Integrated Surface Database (<https://www.ncdc.noaa.gov/isd/data-access>). The surface air pollutants and aerosol species data are provided by Chinese National Environmental Monitoring Center (<http://www.cnemc.cn/en/>) and archived at <https://doi.org/10.6084/m9.figshare.12818807.v1>.

## **References**

- Alexander, B., Hastings, M. G., Allman, D. J., Dachs, J., Thornton, J. A., and Kunasek, S. A.: Quantifying atmospheric nitrate formation pathways based on a global model of the oxygen isotopic composition ( $\delta$  O-17) of atmospheric nitrate, *Atmos Chem Phys*, 9, 5043-5056, 2009.
- Alexander, B., Sherwen, T., Holmes, C. D., Fisher, J. A., Chen, Q. J., Evans, M. J., and Kasibhatla, P.: Global inorganic nitrate production mechanisms: comparison of a global model with nitrate isotope observations, *Atmos Chem Phys*, 20, 3859-3877, 2020.
- Bhati, S. and Mohan, M.: WRF-urban canopy model evaluation for the assessment of heat island and thermal comfort over an urban airshed in India under varying land use/land cover conditions, *Geosci Lett*, 5, doi: 10.1186/s40562-018-0126-7, 2018.

536 Cheng, Y. F., Zheng, G. J., Wei, C., Mu, Q., Zheng, B., Wang, Z. B., Gao, M., Zhang,  
 537 Q., He, K. B., Carmichael, G., Poschl, U., and Su, H.: Reactive nitrogen  
 538 chemistry in aerosol water as a source of sulfate during haze events in China, *Sci*  
 539 *Adv*, 2, e1601530, doi: 10.1126/sciadv.1601530, 2016.

540 Dong, X. Y., Li, J., Fu, J. S., Gao, Y., Huang, K., and Zhuang, G. S.: Inorganic  
 541 aerosols responses to emission changes in Yangtze River Delta, China, *Sci Total*  
 542 *Environ*, 481, 522-532, 2014.

543 Ek, M. B., Mitchell, K. E., Lin, Y., Rogers, E., Grunmann, P., Koren, V., Gayno, G.,  
 544 and Tarpley, J. D.: Implementation of Noah land surface model advances in the  
 545 National Centers for Environmental Prediction operational mesoscale Eta model,  
 546 *J Geophys Res-Atmos*, 108, 8851, doi: 10.1029/2002jd003296, 2003.

547 Fahey, K. M. and Pandis, S. N.: Optimizing model performance: variable size  
 548 resolution in cloud chemistry modeling, *Atmos Environ*, 35, 4471-4478, 2001.

549 Fu, X., Wang, T., Gao, J., Wang, P., Liu, Y. M., Wang, S. X., Zhao, B., and Xue, L.  
 550 K.: Persistent Heavy Winter Nitrate Pollution Driven by Increased  
 551 Photochemical Oxidants in Northern China, *Environ Sci Technol*, 54, 3881-3889,  
 552 2020.

553 Geng, G. N., Zhang, Q., Tong, D., Li, M., Zheng, Y. X., Wang, S. W., and He, K. B.:  
 554 Chemical composition of ambient PM<sub>2.5</sub> over China and relationship to precursor  
 555 emissions during 2005-2012, *Atmos Chem Phys*, 17, 9187-9203, 2017.

556 Gomez-Navarro, J. J., Raible, C. C., and Dierer, S.: Sensitivity of the WRF model to  
 557 PBL parametrisations and nesting techniques: evaluation of wind storms over  
 558 complex terrain, *Geosci Model Dev*, 8, 3349-3363, 2015.

559 Grell, G. A., McKeen, S., Michalakes, J., Bao, J. W., Trainer, M., and Hsie, E. Y.:  
 560 Real-time simultaneous prediction of air pollution and weather during the  
 561 Houston 2000 field experiment, *Fourth Conference on Atmospheric Chemistry:*  
 562 *Urban, Regional And Global Scale Impacts Of Air Pollutants*, 224-227, 2002.

563 Guenther, A., Karl, T., Harley, P., Wiedinmyer, C., Palmer, P. I., and Geron, C.:  
 564 Estimates of global terrestrial isoprene emissions using MEGAN (Model of  
 565 Emissions of Gases and Aerosols from Nature), *Atmos Chem Phys*, 6, 3181-  
 566 3210, 2006.

567 He, H., Wang, Y. S., Ma, Q. X., Ma, J. Z., Chu, B. W., Ji, D. S., Tang, G. Q., Liu, C.,  
 568 Zhang, H. X., and Hao, J. M.: Mineral dust and NO<sub>x</sub> promote the conversion of  
 569 SO<sub>2</sub> to sulfate in heavy pollution days, *Scientific Reports*, 4, 4172, doi:  
 570 10.1038/Srep04172, 2014.

571 He, P. Z., Xie, Z. Q., Yu, X. W., Wang, L. Q., Kang, H., and Yue, F. G.: The  
 572 observation of isotopic compositions of atmospheric nitrate in Shanghai China  
 573 and its implication for reactive nitrogen chemistry, *Sci Total Environ*, 714,  
 574 136727, doi: 10.1016/j.scitotenv.2020.136727, 2020.

575 He, P. Z., Xie, Z. Q., Chi, X. Y., Yu, X. W., Fan, S. D., Kang, H., Liu, C., and Zhan,  
 576 H. C.: Atmospheric Delta O-17(NO<sub>3</sub><sup>-</sup>) reveals nocturnal chemistry dominates  
 577 nitrate production in Beijing haze, *Atmos Chem Phys*, 18, 14465-14476, 2018.

578 Huang, R. J., Zhang, Y. L., Bozzetti, C., Ho, K. F., Cao, J. J., Han, Y. M.,  
 579 Daellenbach, K. R., Slowik, J. G., Platt, S. M., Canonaco, F., Zotter, P., Wolf, R.,  
 580 Pieber, S. M., Bruns, E. A., Crippa, M., Ciarelli, G., Piazzalunga, A.,  
 581 Schwikowski, M., Abbaszade, G., Schnelle-Kreis, J., Zimmermann, R., An, Z. S.,  
 582 Szidat, S., Baltensperger, U., El Haddad, I., and Prevot, A. S. H.: High secondary  
 583 aerosol contribution to particulate pollution during haze events in China, *Nature*,  
 584 514, 218-2222014a.

585 Huang, X., Song, Y., Zhao, C., Li, M. M., Zhu, T., Zhang, Q., and Zhang, X. Y.:  
 586 Pathways of sulfate enhancement by natural and anthropogenic mineral aerosols  
 587 in China, *J Geophys Res-Atmos*, 119, 14165-14179, 2014b.

588 Huang, X., Ding, A., Gao, J., Zheng, B., Zhou, D., Qi, X., Tang, R., Wang, J., Ren, C.,  
 589 Nie, W., Chi, X., Xu, Z., Chen, L., Li, Y., Che, F., Pang, N., Wang, H., Tong, D.,  
 590 Qin, W., Cheng, W., Liu, W., Fu, Q., Liu, B., Chai, F., Davis, S., Zhang, Q., and  
 591 He, K.: Enhanced secondary pollution offset reduction of primary emissions  
 592 during COVID-19 lockdown in China, *Natl Sci Rev*, 1-9, 2020.

593 Iacono, M. J., Delamere, J. S., Mlawer, E. J., Shephard, M. W., Clough, S. A., and  
 594 Collins, W. D.: Radiative forcing by long-lived greenhouse gases: Calculations  
 595 with the AER radiative transfer models, *J Geophys Res-Atmos*, 113, D13103,  
 596 doi: 10.1029/2008jd009944, 2008.



597 Jimenez, P. A., Dudhia, J., Gonzalez-Rouco, J. F., Montavez, J. P., Garcia-  
 598 Bustamante, E., Navarro, J., de Arellano, J. V. G., and Munoz-Roldan, A.: An  
 599 evaluation of WRF's ability to reproduce the surface wind over complex terrain  
 600 based on typical circulation patterns, *J Geophys Res-Atmos*, 118, 7651-7669,  
 601 2013.

602 Kalsoom, U., Wang, T. J., Ma, C. Q., Shu, L., Huang, C. W., and Gao, L. B.:  
 603 Quadrennial variability and trends of surface ozone across China during 2015-  
 604 2018: A regional approach, *Atmos Environ*, 245, 117989, doi:  
 605 10.1016/j.atmosenv.2020.117989, 2021.

606 Lei, H., Wuebbles, D. J.: Chemical competition in nitrate and sulfate formations and  
 607 its effect on air quality, *Atmos Environ*, 80, 472-477, 2013.

608 Li, K., Jacob, D. J., Liao, H., Shen, L., Zhang, Q., and Bates, K. H.: Anthropogenic  
 609 drivers of 2013-2017 trends in summer surface ozone in China, *P Natl Acad Sci*  
 610 *USA*, 116, 422-427, 2019a.

611 Li, M. M., Song, Y., Huang, X., Li, J. F., Mao, Y., Zhu, T., Cai, X. H., and Liu, B.:  
 612 Improving mesoscale modeling using satellite-derived land surface parameters in  
 613 the Pearl River Delta region, China, *J Geophys Res-Atmos*, 119, 6325-6346,  
 614 2014.

615 Li, M. M., Wang, T. J., Shu, L., Qu, Y. W., Xie, M., Liu, J. N., Wu, H., and Kalsoom,  
 616 U.: Rising surface ozone in China from 2013 to 2017: A response to the recent  
 617 atmospheric warming or pollutant controls?, *Atmos Environ*, 246, 118130, doi:  
 618 10.1016/j.atmosenv.2020.118130, 2021a.

619 Li, M. M., Wang, T. J., Xie, M., Zhuang, B. L., Li, S., Han, Y., Song, Y., and Cheng,  
 620 N. L.: Improved meteorology and ozone air quality simulations using MODIS  
 621 land surface parameters in the Yangtze River Delta urban cluster, China, *J*  
 622 *Geophys Res-Atmos*, 122, 3116-3140, 2017.

623 Li, M. M., Wang, T. J., Xie, M., Li, S., Zhuang, B. L., Huang, X., Chen, P. L., Zhao,  
 624 M., and Liu, J. E.: Formation and Evolution Mechanisms for Two Extreme Haze  
 625 Episodes in the Yangtze River Delta Region of China During Winter 2016, *J*  
 626 *Geophys Res-Atmos*, 124, 3607-3623, 2019b.

627 Li, M. M., Wang, T. J., Xie, M., Li, S., Zhuang, B. L., Fu, Q. Y., Zhao, M., Wu, H.,  
 628 Liu, J., Saikawa, E., and Liao, K.: Drivers for the poor air quality conditions in  
 629 North China Plain during the COVID-19 outbreak, *Atmos Environ*, 246, 118103,  
 630 doi: 10.1016/j.atmosenv.2020.118103, 2021b.

631 Lin, Y. L., Farley, R. D., and Orville, H. D.: Bulk Parameterization of the Snow Field  
 632 in a Cloud Model, *J Clim Appl Meteorol*, 22, 1065–1092, 1983.

633 Liu, L., Bei, N. F., Hu, B., Wu, J. R., Liu, S. X., Li, X., Wang, R. N., Liu, Z. R., Shen,  
 634 Z. X., and Li, G. H.: Wintertime nitrate formation pathways in the north China  
 635 plain: Importance of N<sub>2</sub>O<sub>5</sub> heterogeneous hydrolysis, *Environ Pollut*, 266,  
 636 115287, doi: 10.1016/j.envpol.2020.115287, 2020.

637 Liu, M. X., Huang, X., Song, Y., Tang, J., Cao, J. J., Zhang, X. Y., Zhang, Q., Wang,  
 638 S. X., Xu, T. T., Kang, L., Cai, X. H., Zhang, H. S., Yang, F. M., Wang, H. B.,  
 639 Yu, J. Z., Lau, A. K. H., He, L. Y., Huang, X. F., Duan, L., Ding, A. J., Xue, L.  
 640 K., Gao, J., Liu, B., and Zhu, T.: Ammonia emission control in China would  
 641 mitigate haze pollution and nitrogen deposition, but worsen acid rain, *P Natl*  
 642 *Acad Sci USA*, 116, 7760-7765, 2019.

643 Liu, X. H., Zhang, Y., Xing, J., Zhang, Q. A., Wang, K., Streets, D. G., Jang, C.,  
 644 Wang, W. X., and Hao, J. M.: Understanding of regional air pollution over China  
 645 using CMAQ, part II. Process analysis and sensitivity of ozone and particulate  
 646 matter to precursor emissions, *Atmos Environ*, 44, 3719-3727, 2010.

647 Liu, Y. M. and Wang, T.: Worsening urban ozone pollution in China from 2013 to  
 648 2017-Part 2: The effects of emission changes and implications for multi-pollutant  
 649 control, *Atmos Chem Phys*, 20, 6323-6337, 2020.

650 Luo, L., Zhu, R. G., Song, C. B., Peng, J. F., Guo, W., Liu, Y. H., Zheng, N. J., Xiao,  
 651 H. W., and Xiao, H. Y.: Changes in nitrate accumulation mechanisms as PM<sub>2.5</sub>  
 652 levels increase on the North China Plain: A perspective from the dual isotopic  
 653 compositions of nitrate, *Chemosphere*, 263, 127915, doi:  
 654 10.1016/j.chemosphere.2020.127915, 2021.

655 Meng, Z., Dabdub, D., and Seinfeld, J. H.: Chemical coupling between atmospheric  
 656 ozone and particulate matter, *Science*, 277, 116-119, 1997.

657 Nguyen, K. and Dabdub, D.: NO<sub>x</sub> and VOC control and its effects on the formation  
 658 of aerosols, *Aerosol Sci Tech*, 36, 560-572, 2002.

659 Noh, Y., Cheon, W. G., Hong, S. Y., and Raasch, S.: Improvement of the K-profile  
 660 model for the planetary boundary layer based on large eddy simulation data,  
 661 *Bound-Lay Meteorol*, 107, 401–427, 2003.

662 Pathak, R. K., Wang, T., and Wu, W. S.: Nighttime enhancement of PM<sub>2.5</sub> nitrate in  
 663 ammonia-poor atmospheric conditions in Beijing and Shanghai: Plausible  
 664 contributions of heterogeneous hydrolysis of N<sub>2</sub>O<sub>5</sub> and HNO<sub>3</sub> partitioning,  
 665 *Atmos Environ*, 45, 1183-1191, 2011.

666 Pun, B. K. and Seigneur, C.: Sensitivity of particulate matter nitrate formation to  
 667 precursor emissions in the California San Joaquin Valley, *Environ Sci Technol*,  
 668 35, 2979-2987, 2001.

669 Seinfeld, J. H. and Pandis, S. N.: *Atmospheric chemistry and physics: from air*  
 670 *pollution to climate change*. 2nd Edition, John Wiley and Sons, Hoboken, NJ,  
 671 2006.

672 Shao, P. Y., Tian, H. Z., Sun, Y. J., Liu, H. J., Wu, B. B., Liu, S. H., Liu, X. Y., Wu,  
 673 Y. M., Liang, W. Z., Wang, Y., Gao, J. J., Xue, Y. F., Bai, X. X., Liu, W., Lin, S.  
 674 M., and Hu, G. Z.: Characterizing remarkable changes of severe haze events and  
 675 chemical compositions in multi-size airborne particles (PM<sub>1</sub>, PM<sub>2.5</sub> and PM<sub>10</sub> )  
 676 from January 2013 to 2016-2017 winter in Beijing, China, *Atmos Environ*, 189,  
 677 133-144, 2018.

678 Shu, L., Wang, T. J., Xie, M., Li, M. M., Zhao, M., Zhang, M., and Zhao, X. Y.:  
 679 Episode study of fine particle and ozone during the CAPUM-YRD over Yangtze  
 680 River Delta of China: Characteristics and source attribution, *Atmos Environ*, 203,  
 681 87-101, 2019.

682 Silver, B., Reddington, C. L., Arnold, S. R., and Spracklen, D. V.: Substantial  
 683 changes in air pollution across China during 2015-2017, *Environ Res Lett*, 14,  
 684 114012, 2018.

685 Smith, A., Lott, N., and Vose, R.: *The Integrated Surface Database Recent*  
 686 *Developments and Partnerships*, *B Am Meteorol Soc*, 92, 704-708, 2011.

687 Sun, Y. L., Wang, Z. F., Dong, H. B., Yang, T., Li, J., Pan, X. L., Chen, P., and Jayne,  
688 J. T.: Characterization of summer organic and inorganic aerosols in Beijing,  
689 China with an Aerosol Chemical Speciation Monitor, *Atmos Environ*, 51, 250-  
690 259, 2012.

691 Tsimpidi, A. P., Karydis, V. A., and Pandis, S. N.: Response of Fine Particulate  
692 Matter to Emission Changes of Oxides of Nitrogen and-Anthropogenic Volatile  
693 Organic Compounds in the Eastern United States, *J Air Waste Manage*, 58,  
694 1463-1473, 2008.

695 Wang, G. H., Zhang, R. Y., Gomez, M. E., Yang, L. X., Zamora, M. L., Hu, M., Lin,  
696 Y., Peng, J. F., Guo, S., Meng, J. J., Li, J. J., Cheng, C. L., Hu, T. F., Ren, Y. Q.,  
697 Wang, Y. S., Gao, J., Cao, J. J., An, Z. S., Zhou, W. J., Li, G. H., Wang, J. Y.,  
698 Tian, P. F., Marrero-Ortiz, W., Secrest, J., Du, Z. F., Zheng, J., Shang, D. J.,  
699 Zeng, L. M., Shao, M., Wang, W. G., Huang, Y., Wang, Y., Zhu, Y. J., Li, Y. X.,  
700 Hu, J. X., Pan, B., Cai, L., Cheng, Y. T., Ji, Y. M., Zhang, F., Rosenfeld, D., Liss,  
701 P. S., Duce, R. A., Kolb, C. E., and Molina, M. J.: Persistent sulfate formation  
702 from London Fog to Chinese haze, *P Natl Acad Sci USA*, 113, 13630-13635,  
703 2016.

704 Wang, H. C., Lu, K. D., Chen, X. R., Zhu, Q. D., Chen, Q., Guo, S., Jiang, M. Q., Li,  
705 X., Shang, D. J., Tan, Z. F., Wu, Y. S., Wu, Z. J., Zou, Q., Zheng, Y., Zeng, L.  
706 M., Zhu, T., Hu, M., and Zhang, Y. H.: High N<sub>2</sub>O<sub>5</sub> Concentrations Observed in  
707 Urban Beijing: Implications of a Large Nitrate Formation Pathway, *Environ Sci*  
708 *Tech Let*, 4, 416-420, 2017a.

709 Wang, J. D., Zhao, B., Wang, S. X., Yang, F. M., Xing, J., Morawska, L., Ding, A. J.,  
710 Kulmala, M., Kerminen, V. M., Kujansuu, J., Wang, Z. F., Ding, D. A., Zhang,  
711 X. Y., Wang, H. B., Tian, M., Petaja, T., Jiang, J. K., and Hao, J. M.: Particulate  
712 matter pollution over China and the effects of control policies, *Sci Total Environ*,  
713 584, 426-447, 2017b.

714 Wang, S. X., Xing, J., Zhao, B., Jang, C., and Hao, J. M.: Effectiveness of national air  
715 pollution control policies on the air quality in metropolitan areas of China, *J*  
716 *Environ Sci*, 26, 13-22, 2014.

717 Wang, X. F., Wang, W. X., Yang, L. X., Gao, X. M., Nie, W., Yu, Y. C., Xu, P. J.,  
718 Zhou, Y., and Wang, Z.: The secondary formation of inorganic aerosols in the

719 droplet mode through heterogeneous aqueous reactions under haze conditions,  
 720 Atmos Environ, 63, 68-76, 2012.

721 Wang, Y., Zhang, Q. Q., He, K., Zhang, Q., and Chai, L.: Sulfate-nitrate-ammonium  
 722 aerosols over China: response to 2000-2015 emission changes of sulfur dioxide,  
 723 nitrogen oxides, and ammonia, Atmos Chem Phys, 13, 2635-2652, 2013.

724 Wang, Y. L., Song, W., Yang, W., Sun, X. C., Tong, Y. D., Wang, X. M., Liu, C. Q.,  
 725 Bai, Z. P., and Liu, X. Y.: Influences of Atmospheric Pollution on the  
 726 Contributions of Major Oxidation Pathways to PM<sub>2.5</sub> Nitrate Formation in  
 727 Beijing, J Geophys Res-Atmos, 124, 4174-4185, 2019.

728 Wen, L., Xue, L. K., Wang, X. F., Xu, C. H., Chen, T. S., Yang, L. X., Wang, T.,  
 729 Zhang, Q. Z., and Wang, W. X.: Summertime fine particulate nitrate pollution in  
 730 the North China Plain: increasing trends, formation mechanisms and implications  
 731 for control policy, Atmos Chem Phys, 18, 11261-11275, 2018.

732 Wen, Z., Xu, W., Pan, X. Y., Han, M. J., Wang, C., Benedict, K., Tang, A. H., Collet,  
 733 J. L., and Liu, X. J.: Effects of reactive nitrogen gases on the aerosol formation  
 734 in Beijing from late autumn to early spring, Environ Res Lett, 16, 025005, doi:  
 735 10.1088/1748-9326/abd973, 2021.

736 Womack, C. C., McDuffie, E. E., Edwards, P. M., Bares, R., de Gouw, J. A.,  
 737 Docherty, K. S., Dube, W. P., Fibiger, D. L., Franchin, A., Gilman, J. B.,  
 738 Goldberger, L., Lee, B. H., Lin, J. C., Lone, R., Middlebrook, A. M., Millet, D.  
 739 B., Moravek, A., Murphy, J. G., Quinn, P. K., Riedel, T. P., Roberts, J. M.,  
 740 Thornton, J. A., Valin, L. C., Veres, P. R., Whitehill, A. R., Wild, R. J., Warneke,  
 741 C., Yuan, B., Baasandorj, M., and Brown, S. S.: An Odd Oxygen Framework for  
 742 Wintertime Ammonium Nitrate Aerosol Pollution in Urban Areas: NO<sub>x</sub> and  
 743 VOC Control as Mitigation Strategies, Geophys Res Lett, 46, 4971-4979, 2019.

744 Xie, M., Zhu, K. G., Wang, T. J., Yang, H. M., Zhuang, B. L., Li, S., Li, M. G., Zhu,  
 745 X. S., and Ouyang, Y.: Application of photochemical indicators to evaluate  
 746 ozone nonlinear chemistry and pollution control countermeasure in China,  
 747 Atmos Environ, 99, 466-473, 2014.

748 Xue, J., Yuan, Z. B., Lau, A. K. H., and Yu, J. Z.: Insights into factors affecting  
 749 nitrate in PM<sub>2.5</sub> in a polluted high NO<sub>x</sub> environment through hourly

750 observations and size distribution measurements, *J Geophys Res-Atmos*, 119,  
751 4888-4902, 2014.

752 Xue, J., Yuan, Z. B., Griffith, S. M., Yu, X., Lau, A. K. H., and Yu, J. Z.: Sulfate  
753 Formation Enhanced by a Cocktail of High NO<sub>x</sub>, SO<sub>2</sub>, Particulate Matter, and  
754 Droplet pH during Haze-Fog Events in Megacities in China: An Observation-  
755 Based Modeling Investigation, *Environ Sci Technol*, 50, 7325-7334, 2016.

756 Zaveri, R. A. and Peters, L. K.: A new lumped structure photochemical mechanism  
757 for large-scale applications, *J Geophys Res-Atmos*, 104, 30387-30415, 1999.

758 Zaveri, R. A., Easter, R. C., Fast, J. D., and Peters, L. K.: Model for Simulating  
759 Aerosol Interactions and Chemistry (MOSAIC), *J Geophys Res-Atmos*, 113,  
760 D13204, doi: 10.1029/2007jd008782, 2008.

761 Zhai, S. X., Jacob, D. J., Wang, X., Shen, L., Li, K., Zhang, Y. Z., Gui, K., Zhao, T.  
762 L., and Liao, H.: Fine particulate matter (PM<sub>2.5</sub>) trends in China, 2013-2018:  
763 separating contributions from anthropogenic emissions and meteorology, *Atmos*  
764 *Chem Phys*, 19, 11031-11041, 2019.

765 Zhang, W. Q., Tong, S. R., Ge, M. F., An, J. L., Shi, Z. B., Hou, S. Q., Xia, K. H., Qu,  
766 Y., Zhang, H. X., Chu, B. W., Sun, Y. L., and He, H.: Variations and sources of  
767 nitrous acid (HONO) during a severe pollution episode in Beijing in winter 2016,  
768 *Sci Total Environ*, 648, 253-262, 2019.

769 Zhang, Y. M., Wang, Y. Q., Zhang, X. Y., Shen, X. J., Sun, J. Y., Wu, L. Y., Zhang,  
770 Z. X., and Che, H. C.: Chemical Components, Variation, and Source  
771 Identification of PM<sub>1</sub> during the Heavy Air Pollution Episodes in Beijing in  
772 December 2016, *J Meteorol Res-Prc*, 32, 1-13, 2018.

773 Zhao, M. F., Xiu, G. L., Qiao, T., Li, Y. L., and Yu, J. Z.: Characteristics of Haze  
774 Pollution Episodes and Analysis of a Typical Winter Haze Process in Shanghai,  
775 *Aerosol Air Qual Res*, 16, 1625-1637, 2016.

776 Zhao, P. S., Dong, F., He, D., Zhao, X. J., Zhang, X. L., Zhang, W. Z., Yao, Q., and  
777 Liu, H. Y.: Characteristics of concentrations and chemical compositions for  
778 PM<sub>2.5</sub> in the region of Beijing, Tianjin, and Hebei, China, *Atmos Chem Phys*,  
779 13, 4631-4644, 2013.

780 Zheng, B., Tong, D., Li, M., Liu, F., Hong, C. P., Geng, G. N., Li, H. Y., Li, X., Peng,  
781 L. Q., Qi, J., Yan, L., Zhang, Y. X., Zhao, H. Y., Zheng, Y. X., He, K. B., and  
782 Zhang, Q.: Trends in China's anthropogenic emissions since 2010 as the  
783 consequence of clean air actions, *Atmos Chem Phys*, 18, 14095-14111, 2018.

784

785

**Table 1.** The emission scenarios in WRF-Chem numerical experiments

Simulation scenarios	Descriptions
B0	Base simulation under the 2016 emission conditions.
$C_N$ ( $N=1/2/\dots/8$ )	Same as B0, but anthropogenic $\text{NO}_x$ emissions are reduced by 10%, 20%...80%, respectively, relative to the usual levels in 2016.
$C_{S-N}$ ( $N=2/4/6/8$ )	Same as B0, but anthropogenic $\text{SO}_2$ emissions are reduced by 20%, 40%...80%, respectively, relative to the usual levels in 2016.
$C_{N-N}$ ( $N=2/4/6/8$ )	Same as B0, but anthropogenic $\text{NH}_3$ emissions are reduced by 20%, 40%...80%, respectively, relative to the usual levels in 2016.
$C_{V-N}$ ( $N=2/4/6/8$ )	Same as B0, but anthropogenic $\text{VOC}_s$ emissions are reduced by 20%, 40%...80%, respectively, relative to the usual levels in 2016.
N0	Same as B0, but only consider the $\text{NO}_2+\text{OH}$ gas-phase oxidation pathway for the production of nitrate aerosol.
E1	Same as B0, but anthropogenic $\text{NO}_x$ emissions are replaced using the MEIC inventory in 2012.

786

787

**Table 2.** Statistical evaluations of the model meteorological performance

Variable	Obs	Sim	$R^a$	MB <sup>a</sup>	NMB <sup>a</sup>	ME <sup>a</sup>	RMSE <sup>a</sup>
Period I (15 August to 16 September)							
Temperature ( $^{\circ}\text{C}$ )	24.04	23.91	0.89	-0.13	-0.55%	1.98	2.63
Humidity (%)	70.89	66.88	0.78	-4.01	-5.65%	11.07	14.67
Wind speed ( $\text{m s}^{-1}$ )	2.46	3.04	0.50	0.58	23.72%	1.38	1.83
Period II (24 November to 26 December)							
Temperature ( $^{\circ}\text{C}$ )	3.43	3.40	0.94	-0.03	-0.80%	2.18	2.83
Humidity (%)	69.85	65.27	0.63	-4.58	-6.56%	13.51	17.88
Wind speed ( $\text{m s}^{-1}$ )	2.61	3.66	0.55	1.06	40.64%	1.70	2.23

788

<sup>a</sup>  $R$ : correlation efficient; MB: mean bias; NMB: normalized mean bias; ME: mean

789

error; RMSE: root mean square error.

790

791

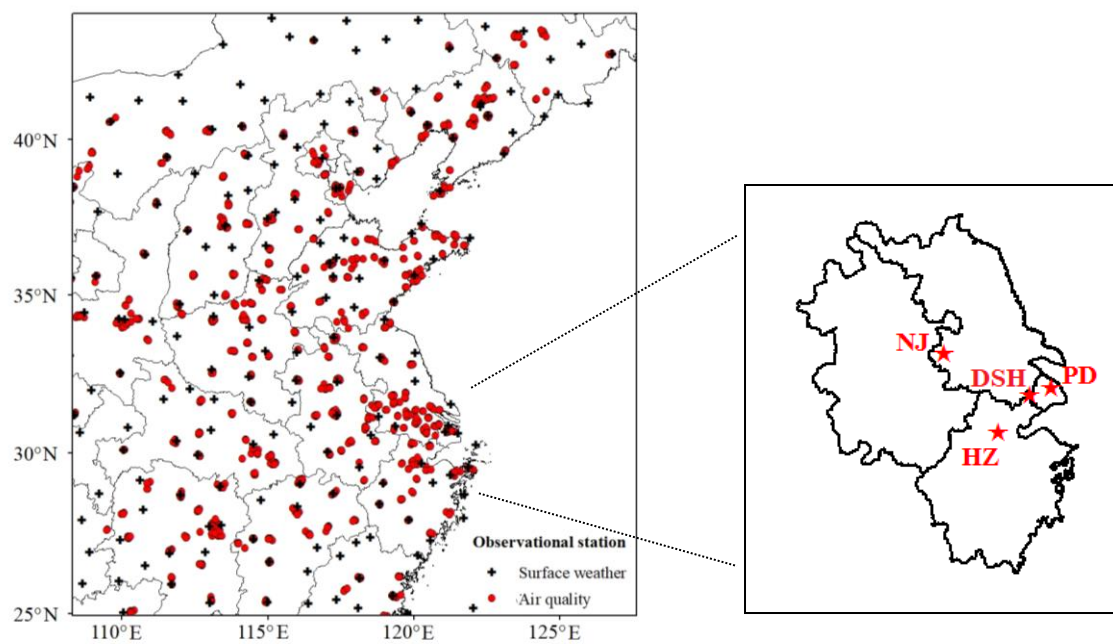


792

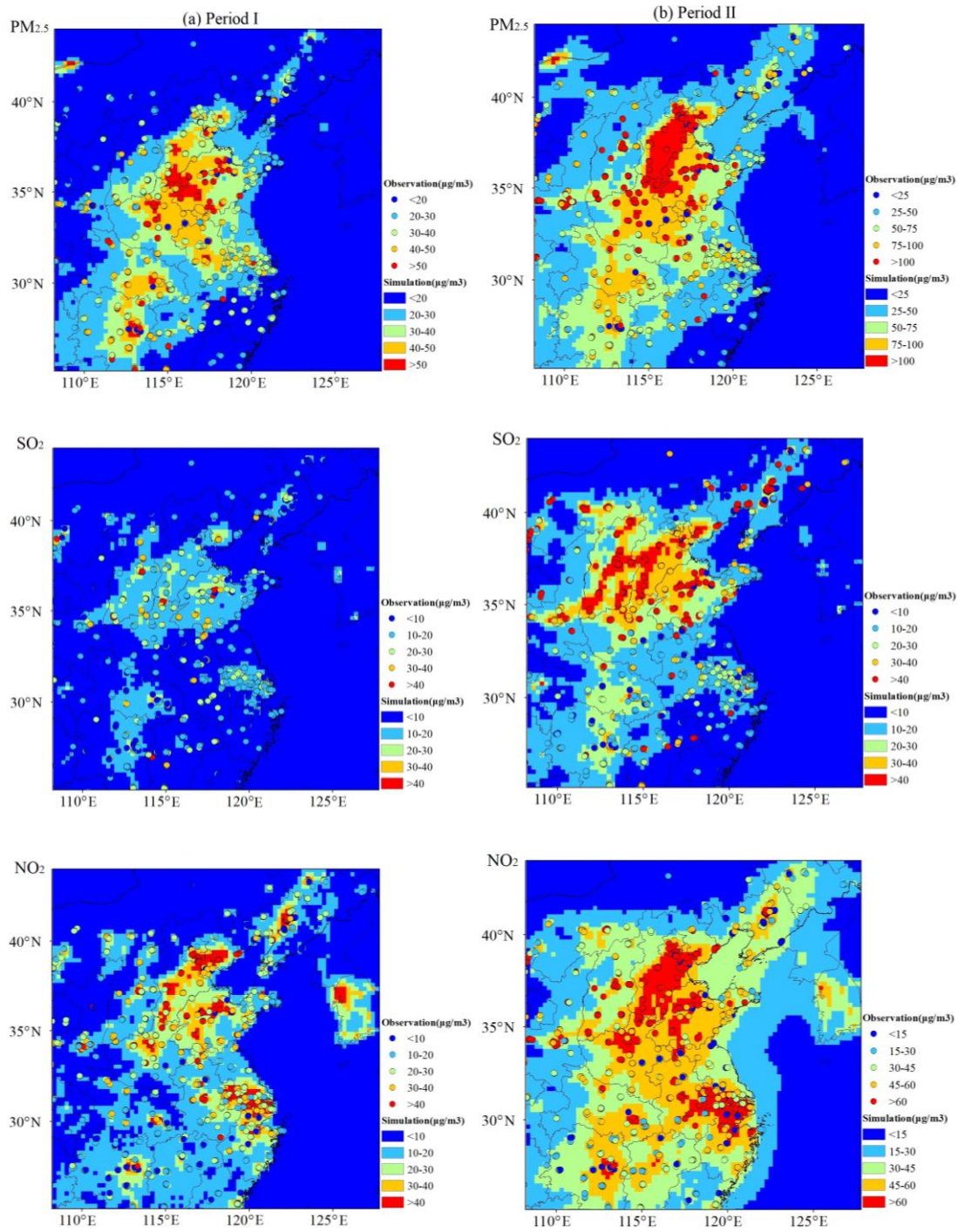
**Table 3.** Statistical evaluations of the model chemical performance

Variable	Obs	Sim	MB	NMB	Obs	Sim	MB	NMB
Period I				Period II				
PM <sub>2.5</sub>	36.88	33.22	−3.66	−9.92%	91.59	64.28	−27.31	−29.82%
SO <sub>2</sub>	17.65	16.51	−1.14	−6.46%	41.45	29.80	−11.65	−28.11%
NO <sub>2</sub>	28.53	33.23	4.70	16.47%	53.01	54.28	1.27	2.40%
Daily- maximum O <sub>3</sub>	237.45	255.77	18.32	7.72%	125.62	86.61	−39.01	−31.05%

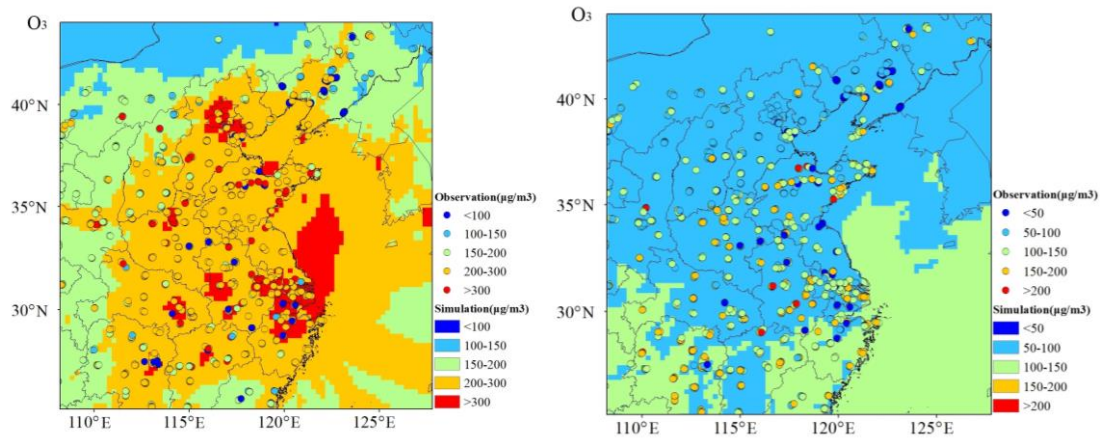
793



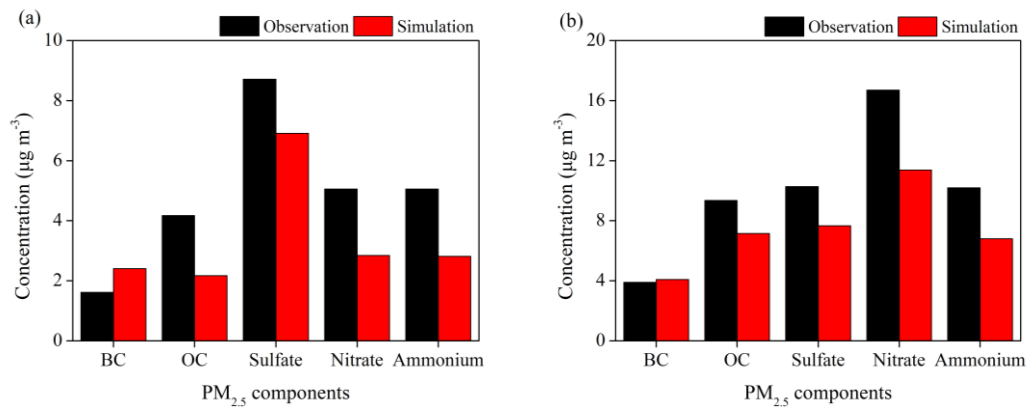
**Fig. 1.** WRF-Chem domain configuration and observational stations. Black crosses:  
 surface weather stations; Red dots: CNEMC routine air quality monitoring stations;  
 Red stars: surface supersites in YRD.



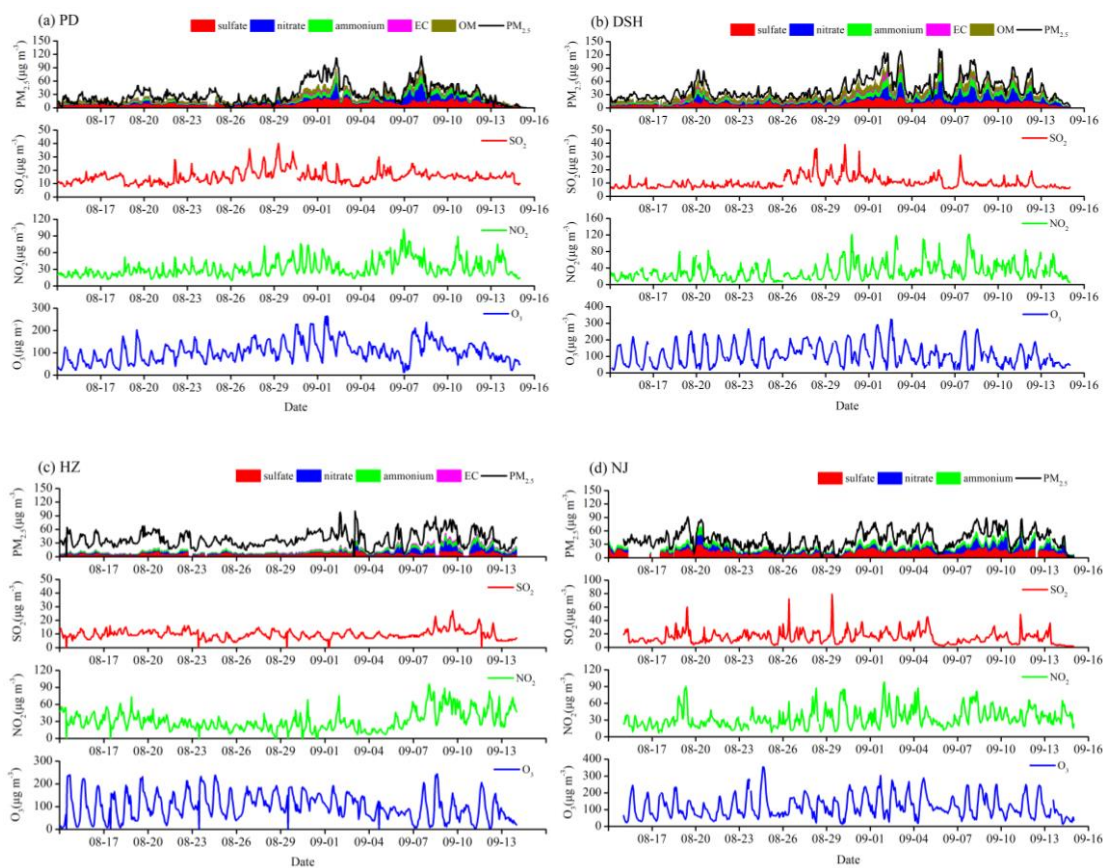
**Fig. 2.** Spatial patterns of the surface average PM<sub>2.5</sub>, NO<sub>2</sub>, SO<sub>2</sub> and daily-maximum O<sub>3</sub> concentrations in Period I (left panels) and Period II (right panels) from the WRF-Chem modeling (shaded contours) and routine air quality observations (dots).



**Fig. 2.** Continued.

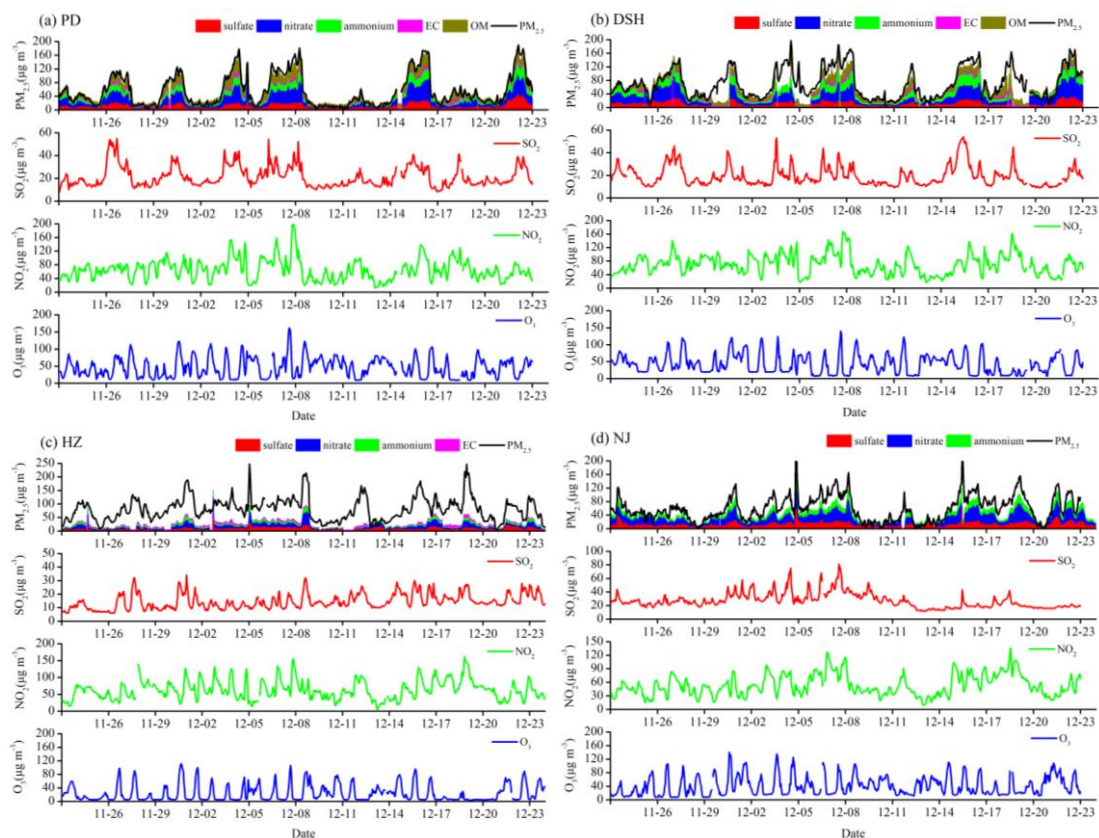


**Fig. 3.** Comparisons of surface PM<sub>2.5</sub> components from WRF-Chem simulations and observations in Period I (a) and Period II (b) at the four supersites in YRD.

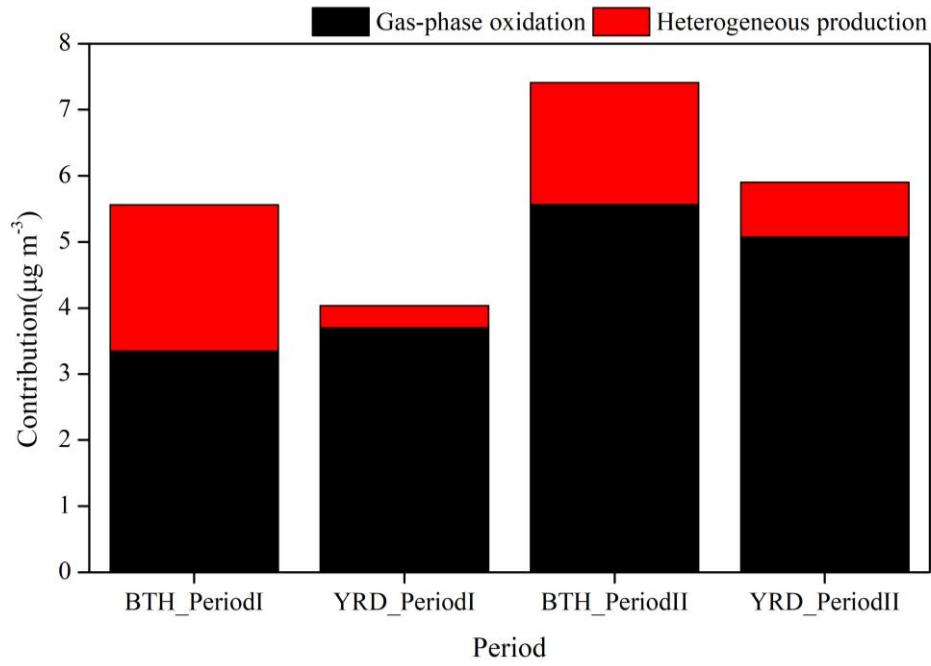


**Fig. 4.** Observed aerosol composition and gaseous pollutants concentrations at the four supersites during Period I.

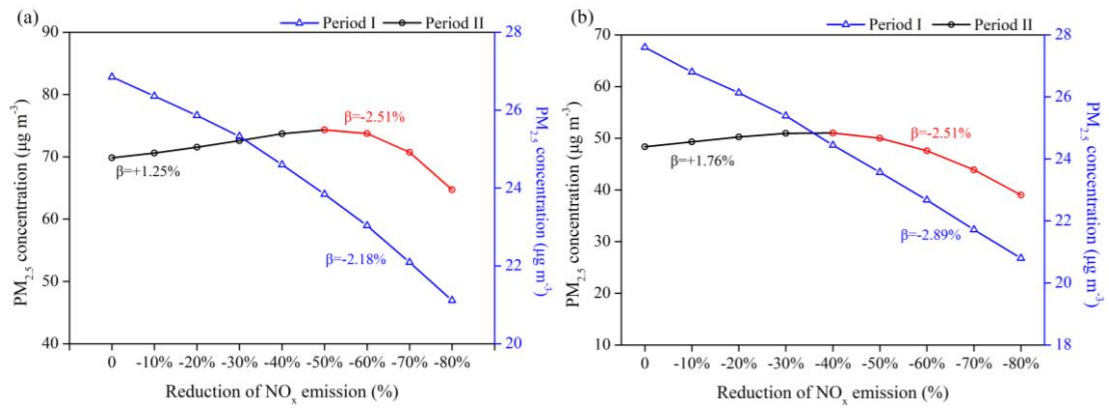




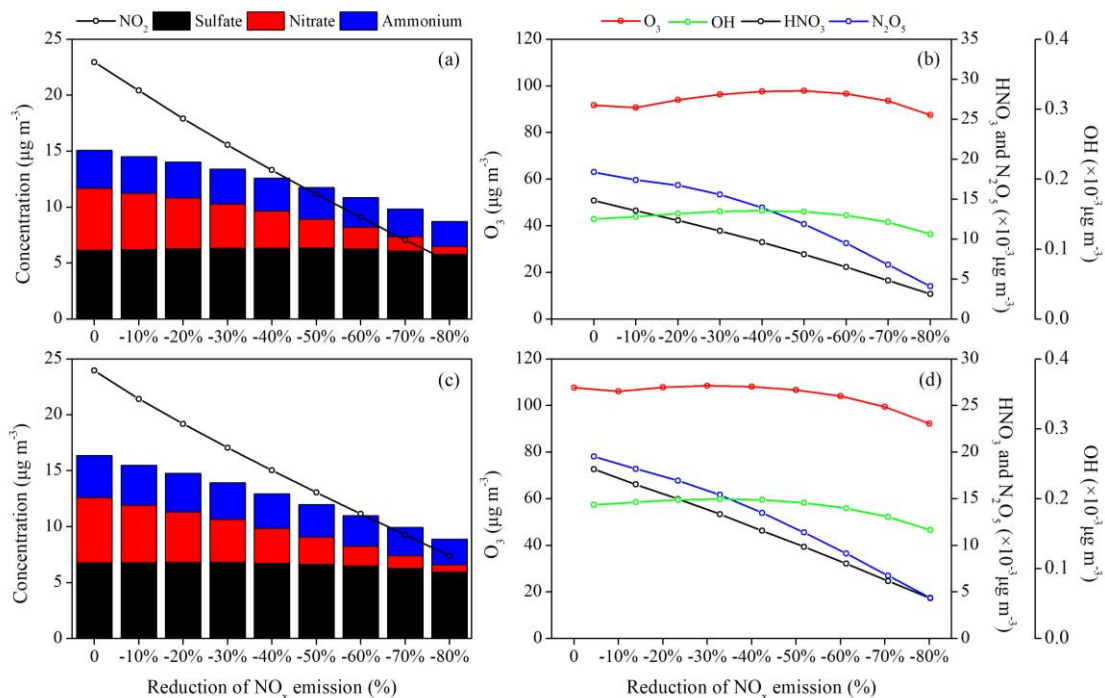
**Fig. 5.** Same as Fig. 4, but for Period II.



**Fig. 6.** Contributions of gas-phase oxidation and heterogeneous production to the surface nitrate concentrations for the BTH and YRD regions in two seasons.

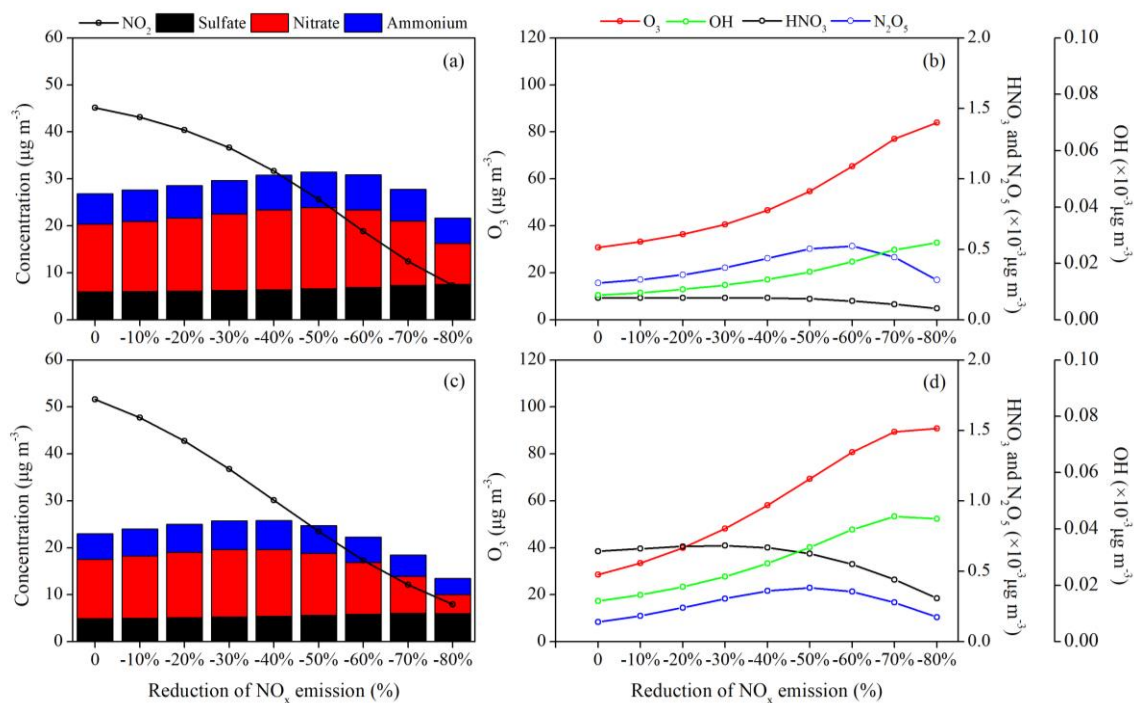


**Fig. 7.** Responses of surface PM<sub>2.5</sub> concentrations to the NO<sub>x</sub> emission reduction scenarios in (a) BTH and (b) YRD. The calculated NO<sub>x</sub> emission control efficiency ( $\beta$ ) is also marked in the figure.



826

**Fig. 8.** Responses of the surface concentrations of SIA components and key atmospheric trace gases (NO<sub>2</sub>, O<sub>3</sub>, OH, HNO<sub>3</sub> and NO<sub>3</sub>) to the NO<sub>x</sub> emission reduction scenarios in (a, b) BTH and (c, d) YRD during Period I.

830  
831

**Fig. 9.** Same as Fig. 8, but for Period II.



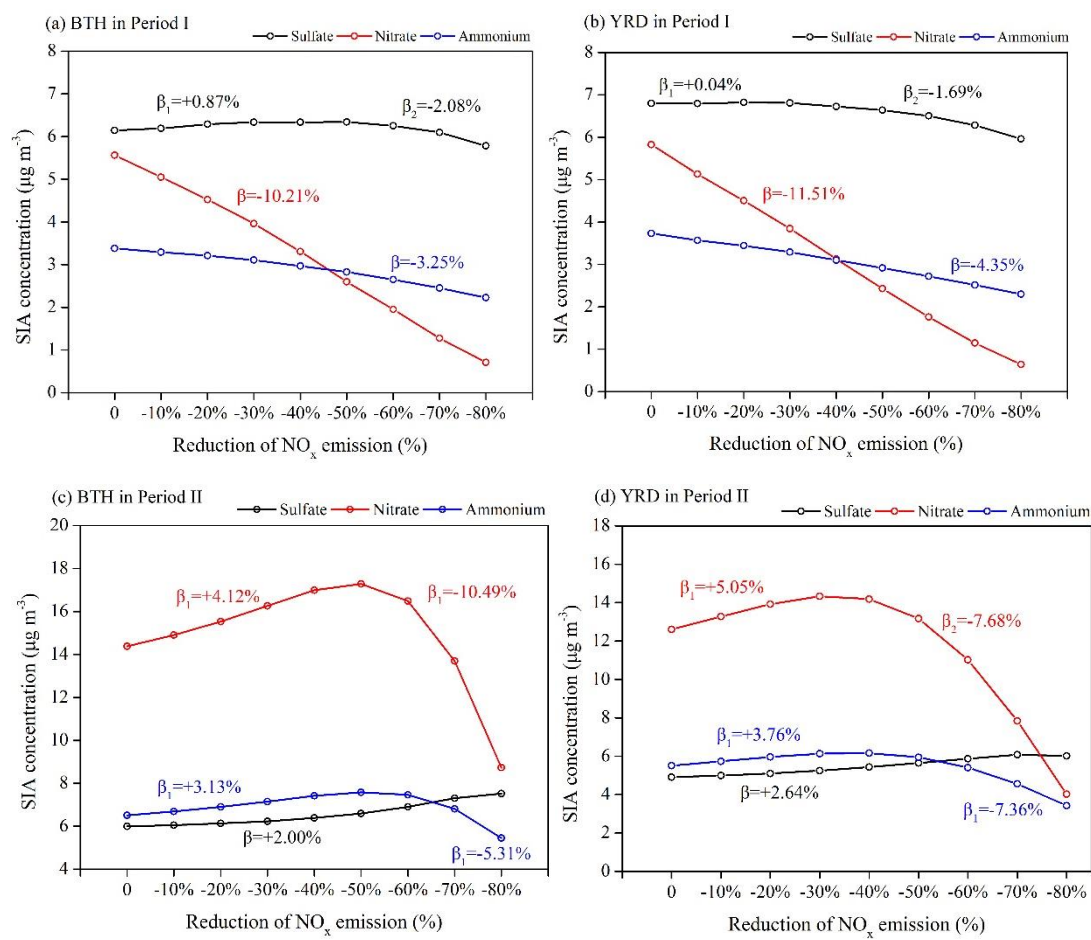


**Fig. 10.** Responses of the surface concentrations of SIA components to the  $\text{NO}_x$  emission reduction scenarios and their emission control efficiencies in (a, b) Period I and (c, d) Period II.

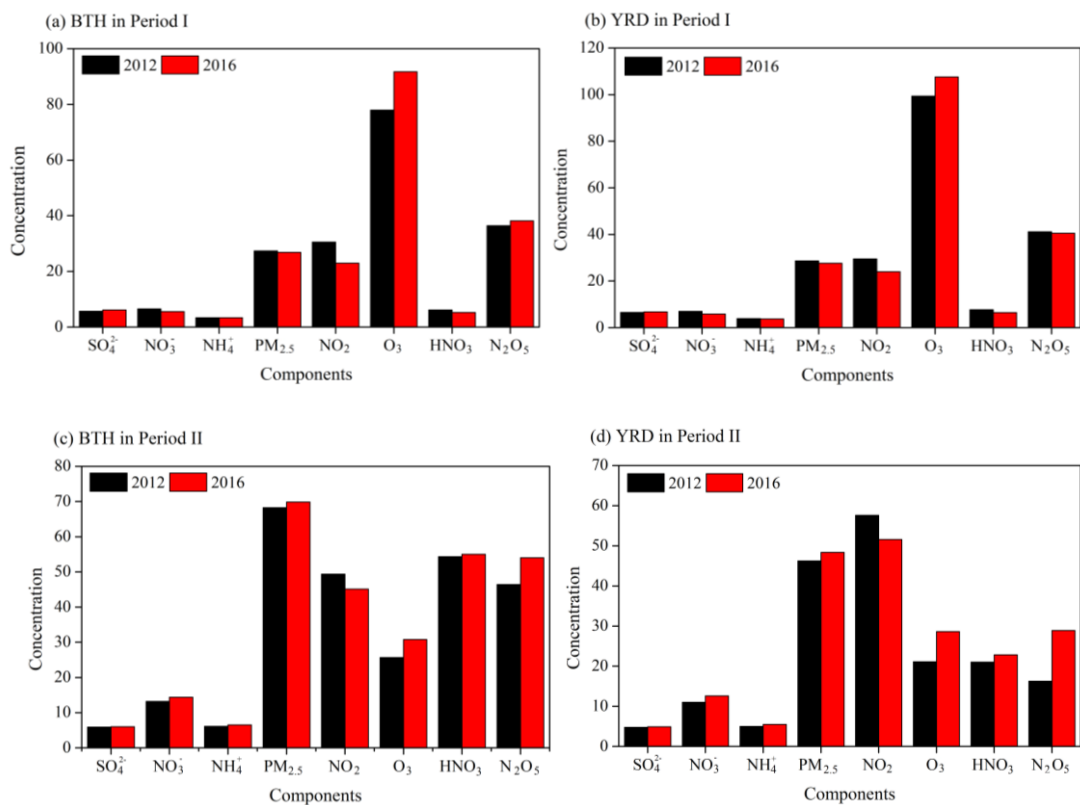


**Fig. 11.** Changes in the concentrations of surface  $\text{PM}_{2.5}$ , SIA components and key atmospheric trace ( $\text{NO}_2$ ,  $\text{O}_3$ ,  $\text{HNO}_3$  and  $\text{N}_2\text{O}_5$ ) due to the 2012–2016  $\text{NO}_x$  emission reductions in China estimated as the differences between the base simulation and E1 scenario. The units are ppt for  $\text{HNO}_3$  and  $\text{N}_2\text{O}_5$ , and  $\mu\text{g m}^{-3}$  for other chemical species.

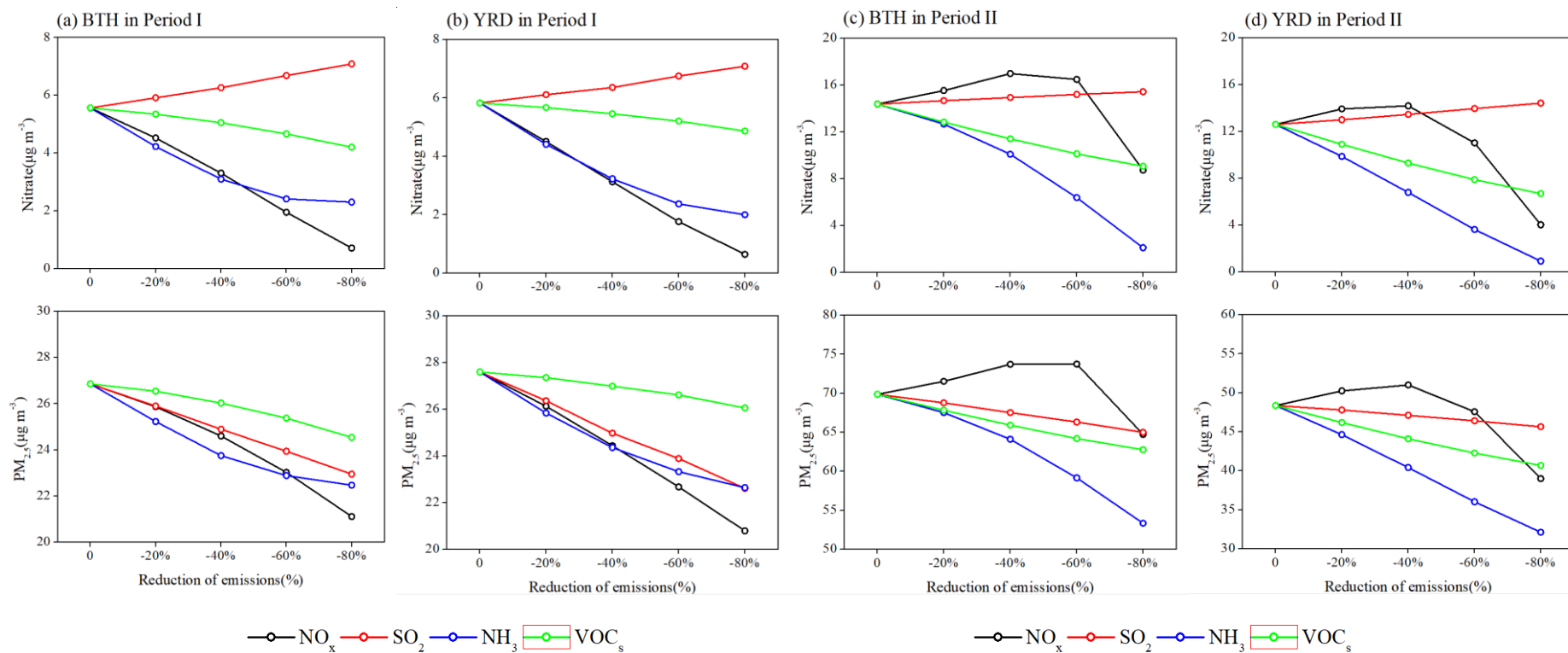


**Fig. 12.** Responses of the surface nitrate (upper panels) and PM<sub>2.5</sub> (bottom panels) concentrations to the emission reduction scenarios of NO<sub>x</sub>, SO<sub>2</sub>, NH<sub>3</sub> and VOC<sub>s</sub> during Period I (a, b) and Period II (c, d).